Antibody evasion by the Brazilian P.1 strain of SARS-CoV-2

Wanwisa Dejnirattisai[#,1], Daming Zhou [#,2], Piyada Supasa[#,1], Chang Liu[#,1,3], Alexander J. Mentzer[#,1,4], Helen M. Ginn[5], Yuguang Zhao[2], Helen M.E. Duyvesteyn[2], Aekkachai Tuekprakhon[1], Rungtiwa Nutalai[1], Beibei Wang[1], Guido C. Paesen[2], César López-Camacho[1], Jose Slon-Campos[1], Thomas S. Walter[2], Donal Skelly[4,6,7], Sue Ann Costa Clemens[8], Felipe Gomes Naveca[9], Valdinete Nascimento[9], Fernanda Nascimento[9], Cristiano Fernandes da Costa[10], Christina Dold[11,12], Robert Levin[13], Tao Dong[3,14,15], Andrew J. Pollard[11,12], Julian C. Knight[1,4], Derrick Crook[15], Teresa Lambe[16], Elizabeth Clutterbuck[11,12], Sagida Bibi[11,12], Amy Flaxman[16], Mustapha Bittaye[16], Sandra Belij-Rammerstorfer[16], Sarah Gilbert[16], Miles W. Carroll[1,17], Paul Klenerman[4,6,11,18], Eleanor Barnes[4,6,11,18], Susanna J. Dunachie[4,6,19,20], Neil G. Paterson[5], Mark A. Williams[5], David R. Hall[5], Ruben J. G. Hulswit[2], Thomas A. Bowden[2], Elizabeth E. Fry[2], Juthathip Mongkolsapaya[$,1,3,21], Jingshan Ren[$,2], David I. Stuart[$,1,2,3,5,22], Gavin R. Screaton[$,1,3]

1. Wellcome Centre for Human Genetics, Nuffield Department of Medicine, University of Oxford, Oxford, UK.
2. Division of Structural Biology, Nuffield Department of Medicine, University of Oxford, The Wellcome Centre for Human Genetics, Oxford, UK.
3. Chinese Academy of Medical Science (CAMS) Oxford Institute (COI), University of Oxford, Oxford, UK.
4. Oxford University Hospitals NHS Foundation Trust, Oxford, UK.
5. Diamond Light Source Ltd, Harwell Science & Innovation Campus, Didcot, UK.
6. Peter Medawar Building for Pathogen Research, Oxford, UK.
7. Nuffield Department of Clinical Neurosciences, University of Oxford, Oxford, UK
8. Institute of Global Health, University of Siena, Siena, Brazil; Department of Paediatrics, University of Oxford, Oxford, UK.
9. Laboratório de Ecologia de Doenças Transmissíveis na Amazônia, Instituto Leônidas e Maria Deane, Fiocruz, Manaus, Amazonas, Brazil.
10. Fundação de Vigilância em Saúde do Amazonas, Manaus, Amazonas, Brazil
11.NIHR Oxford Biomedical Research Centre, Oxford, UK.
12. Oxford Vaccine Group, Department of Paediatrics, University of Oxford, Oxford, UK.
13. Worthing Hospital, Worthing, UK.
14. MRC Human Immunology Unit, MRC Weatherall Institute of Molecular Medicine, Radcliffe Department of Medicine, University of Oxford, Oxford, UK.
15. Nuffield Department of Medicine, University of Oxford, Oxford, UK.
16. Jenner Institute, Nuffield Department of Medicine, University of Oxford, Oxford, UK.
17. National Infection Service, Public Health England (PHE), Porton Down, Salisbury, UK..
18. Translational Gastroenterology Unit, University of Oxford, Oxford, UK
19. Centre For Tropical Medicine and Global Health, Nuffield Deptment of Medicine, University of Oxford, Oxford, UK.
20. Mahidol-Oxford Tropical Medicine Research Unit, Bangkok, Thailand.
Department of Medicine, University of Oxford, Oxford, UK.
21. Siriraj Center of Research Excellence in Dengue & Emerging Pathogens, Dean Office for Research, Faculty of Medicine Siriraj Hospital, Mahidol University, Thailand.
22. Instruct-ERIC, Oxford House, Parkway Court, John Smith Drive, Oxford, UK.

# These authors contributed equally to this work.
$ corresponding authors

Summary

Terminating the SARS-CoV-2 pandemic relies upon pan-global vaccination. Current vaccines elicit neutralizing antibody responses to the virus spike derived from early isolates. However, new strains have emerged with multiple mutations: P.1 from Brazil, B.1.351 from South Africa and B.1.1.7 from the UK (12, 10 and 9 changes in the spike respectively). All have mutations in the ACE2 binding site with P.1 and B.1.351 having a virtually identical triplet: E484K, K417N/T and N501Y, which we show confer similar increased affinity for ACE2. We show that, surprisingly, P.1 is significantly less resistant to naturally acquired or vaccine induced antibody responses than B.1.351 suggesting that changes outside the RBD impact neutralisation. Monoclonal antibody 222 neutralises all three variants despite interacting with two of the ACE2 binding site mutations, we explain this through structural analysis and use the 222 light chain to largely restore neutralization potency to a major class of public antibodies.

Introduction

For more than a year SARS-CoV-2 has caused enormous global dislocation, leading to more than 2.5 million deaths (https://www.worldometers.info/coronavirus Accessed: 2021-03-01) and leaving no country untouched. Successive waves of infection have led to the imposition of draconian lock downs in many countries resulting in severe economic and societal disruption (Donthu and Gustafsson, 2020).

Enormous investment has been made in vaccine development with hundreds of vaccine candidates in different stages of development using an array of different platforms from RNA,

viral vectors, recombinant protein and inactivated (Krammer, 2020). Five vaccines have now been through large scale phase III trials and have demonstrated safety and efficacy (Polack et al., 2020;Voysey et al., 2020;Baden et al., 2020). Four of these, BNT162b2 (Pfizer-BioNTech; mRNA), mRNA-1273 (Moderna; mRNA), ChAdOx1 nCoV-19 (AZD1222) (Oxford-AstraZeneca; chimpanzee adenoviral vectored) and Ad26.COV2-S (Janssen; adenovirus serotype 26 vectored) have received emergency use authorization (EUA) in a variety of countries and are being rolled out at massive scale and NVX-CoV2373 (Novavax; recombinant protein) has also shown impressive efficacy and is likely to achieve EUA in the near future (https://www.medscape.com/viewarticle/944933 Accessed: 2021-03-01). All of these vaccines have been designed to raise antibodies (and T-cells) to spike protein (S) and because of the speed of development they all include S sequences derived from the first reported sequence from Wuhan in January 2020 (Lu et al., 2020).

SARS-CoV-2 like all RNA viruses has an error prone RNA polymerase, and despite some error correction, progressive accrual of mutational changes is inevitable. The massive scale of the pandemic which is largely uncontrolled leads to huge levels of viral replication, increasing the chances that adaptive mutations will occur. There are many possible ways whereby a mutation in SARS-CoV-2 may give the virus a selective advantage, however concentrating on mutation in S, there are two clear possibilities: increased efficiency of transmission and escape from neutralizing antibodies (Volz et al., 2021).

The S protein is a large Type-1 transmembrane glycoprotein which assembles into homo-trimers (Walls et al., 2020), which form most of the outer surface of coronaviruses. S is divided into two portions S1 and S2 which are cleaved by proteolysis. S1 is responsible for target cell engagement, whilst S2 completes membrane fusion allowing the viral RNA access to the host

104 cell cytoplasm where viral replication can begin. S1 contains an N terminal domain (NTD) and
105 receptor binding domain (RBD).
106
107 The RBD interacts with the cellular receptor angiotensin converting enzyme-2 (ACE2) which
108 is expressed on diverse cell types, including cells in the upper and lower respiratory tracts,
109 allowing SARS-CoV-2 to cause respiratory infection. The ACE2 interaction surface is a small
110 25 amino acid patch at the apex of spike, presented to ACE2 when the RBD swings upwards
111 (Hoffmann et al., 2020;Shang et al., 2020) and it is mutations in this region that are causing the
112 most concern. Three multiply mutated viral strains appeared independently at the end of 2020
113 in different regions where they rapidly expanded to become the dominant strains
114 (https://www.cogconsortium.uk/wp-content/uploads/2021/01/Report-2_COG-UK_SARS-
115 CoV-2-Mutations.pdf). It is not clear how these strains acquired so many changes without clear
116 intermediate variants. It has however been speculated, with some evidence, that they may have
117 evolved in immunosuppressed chronically infected patients (Kemp et al., 2021) who support
118 high levels of viral replication for months and may be treated with immune plasma or
119 monoclonal antibodies which may drive selection of variants displaying mutations that evade
120 antibody responses.
121
122 Of most concern are changes in the RBD. P.1 has three: K417T, E484K and N501Y, B.1.351
123 also has three: K417N, E484K and N501Y whereas, B.1.1.7 contains the single N501Y
124 mutation. All of these changes have the potential to modulate ACE2/RBD affinity potentially
125 leading to increased transmissibility, for which there is now good evidence in B.1.1.7. In
126 addition, these mutated residues also have the potential to modulate neutralization of SARS-
127 CoV-2 by naturally or vaccine induced antibody responses.
128

129 In this paper we examine an isolate of P.1 cultured from a throat swab taken from an infected
130 patient in Manaus, Brazil in December 2020 and compare its interactions with serum and
131 antibodies with those of three other viruses, an early isolate, B.1.1.7 and B.1.351. We test the
132 ability of immune sera induced by infection with early strains of SARS-CoV-2 (Dejnirattisai
133 et al., 2021), or by vaccination with the Oxford-AstraZenca or Pfizer-BioNTech vaccines to
134 neutralize P.1 (Supasa et al., 2021;Zhou et al., 2021). We see a reduction in the neutralizing
135 capacity of immune serum to P.1 similar to the reduction seen with B.1.1.7, but not as severe
136 as that seen with B.1.351 (Zhou et al., 2021). We demonstrate an increased affinity of P.1 RBD
137 for ACE2 and investigate the structural basis of this through crystallography. We also study
138 neutralization by a panel of potent monoclonal antibodies which block RBD/ACE2 interaction
139 and provide a crystallographic solution of how one potent antibody, mAb 222, of the panel
140 (Dejnirattisai et al., 2021) which contacts both K417 and N501, is resistant to the 501Y and
141 417T/N mutations found in the P.1/B1.351 strains. We dissect the basis for this via a series of
142 high resolution structures of RDB-Fab complexes and based on this restore neutralization of
143 certain antibodies by swapping the light chain. Finally, we bring together data on P.1, B.1.351
144 and B.1.1.7 and attempt to interpret the different effects these have upon the neutralizing
145 capacity of serum generated to early SARS-CoV-2 strains.
146
147 **Results**
148
149 *The P.1 lineage*
150 P.1 was first reported in December 2020 from Manaus in Amazonas province of Northern
151 Brazil (Faria et al., 2021). A large first wave of infection was seen in Manaus in March-June
152 2020 and by October around 75% of individuals from the region are estimated to have been
153 infected, representing a very high attack rate. A second large wave of infection began in

154 December 2020 leading to further hospitalizations. This second wave corresponded with the
155 rapid emergence of P.1, not seen before December when it was found in 52% of cases, rising
156 to 85% by January 2021 (**Figure S1**).
157
158 P.1 contains multiple changes compared to B.1.1.28 and P.2 which had been previously
159 circulating in Brazil (Faria et al., 2021). Compared to the Wuhan sequence P.1 contains the
160 following mutations: L18F, T20N, P26S, D138Y, R190S in the NTD, K417T, E484K, N501Y
161 in the RBD, D614G and H655Y at the C-terminus of S1 and T1027I, V1176F in S2. The
162 position of the changes seen in P.1 compared with those found in B.1.1.7 and B.1.351 together
163 with a representation on where they occur on the full spike protein and RBD are shown in
164 **Figure 1**. Mutations K417T, E484K, N501Y in the ACE2 interacting surface are of the greatest
165 concern because of their potential to promote escape from the neutralizing antibody response
166 which predominately targets this region (**Figure 1D)** (Dejnirattisai et al., 2021). We searched
167 the COVID-19 genomics UK (COG-UK) (Tatusov et al., 2000) and the global initiative on
168 sharing avian influenza data (GISAID) (https://www.gisaid.org) databases. A small number
169 of sequences including the K417T mutation, inclusive of the P.1 lineage, have been observed
170 in sequencing from Japan, France, Belgium, Italy, the Netherlands and Colombia (**Figure S1**).
171
172 It is noteworthy that P.1, B.1.1.7 and B.1.351 have accrued multiple mutations in the NTD, in
173 B.1.1.7 there are two deletions Δ69-70 and Δ144, in B.1.351 four amino acid changes and the
174 Δ242–244 deletion, while in P.1 there are 6 amino acid changes in the NTD but no deletions.
175 Of note, two of the NTD changes in P.1 introduce N-linked glycosylation sequons T20N (TRT
176 to NRT) and R190S (NLR to NLS, **Figure 1E)**. The NTD, in the absence of these changes,
177 reasonably well populated with glycosylation sites, indeed it has been suggested that a single
178 bare patch surrounded by N-linked glycans glycans attached at N17, N74, N122, and N149

179 defines a 'supersite' limiting where neutralizing antibodies can attach to the NTD (Cerutti et
180 al., 2021). Residue 188 is somewhat occluded whereas residue 20 is highly exposed, is close
181 to the site of attachment of neutralizing antibody 159 (Dejnirattisai et al., 2021) and impinges
182 on the proposed NTD supersite.
183
184 *The effects of RBD mutations on ACE2 affinity.*
185 We have previously measured the affinity of RBD/ACE2 interaction for Wuhan, B.1.1.7
186 (N501Y) and B.1.351 (K417N, E484K, N501Y) RBDs. N501Y increased affinity 7-fold and
187 the combination of 417, 484 and 501 mutations further increased affinity (19-fold compared to
188 Wuhan). Here we have expressed P.1 RBD (K417T, E484K, N501Y). The K_D for the
189 P.1/ACE2 interaction is 4.8 nM with Kon=1.08E5/Ms, Koff=5.18E-4/s (**Figure S2**, Methods),
190 showing that binding to P.1 is essentially indistinguishable from B.1.351 (4.0 nM).
191
192 To better understand RBD-ACE2 interactions we determined the crystal structure of the RBD-
193 ACE2 complex at 3.1 Å resolution (Methods, **Table S1**). As expected the mode of RBD-ACE2
194 engagement is essentially identical for P.1 and the original Wuhan RBD sequence (**Figure**
195 **2A**). The RMS deviation between the 791 Ca positions is 0.4 Å, similar to the experimental
196 error in the coordinates, and the local structure around each of the three mutations is conserved.
197 Nevertheless, calculation of the electrostatic potential of the contact surfaces reveals a marked
198 change, with much greater complementarity for the P.1 RBD consistent with higher affinity.
199 (**Figure 2B,C,D**).
200
201 Residue 417 lies at the back of the RBD neck (our RBD anatomy follows Dejnirattisai et al.,
202 2021) and in the original SARS-CoV-2 is a lysine residue which forms a salt-bridge with D30
203 of ACE2 (**Figure 2E**). The threonine of P.1 RBD no longer forms this interaction and the gap

204 created is open to solvent, so there is no obvious reason why the mutation would increase
205 affinity for ACE2, and this is consistent with directed evolution studies (Zahradník et al., 2021)
206 where this mutation was rarely selected in RBDs with increased affinity for ACE2.
207
208 Residue 484 lies atop the left shoulder of the RBD and neither the original Glu nor the Lys of
209 P1 make significant contact with ACE2, nevertheless the marked change in charge
210 substantially improves the electrostatic complementarity (**Figure 2F,G**), consistent with
211 increased affinity.
212
213 Residue 501 lies on the right shoulder of the RBD and the change from a relatively short Asn
214 sidechain to the large aromatic Tyr allows for favourable ring stacking interactions consistent
215 with increased affinity (**Figure 2H**).
216
217 *Binding of P.1 RBD by potent human monoclonal antibodies*
218 We have previously described a large panel of monoclonal antibodies generated from patients
219 infected with early strains of SARS-CoV-2, before the emergence of B.1.1.7 (Dejnirattisai et
220 al., 2021). From this panel we have selected 20 potent antibodies which have focus reduction
221 neutralization 50% (FRNT50) values <100ng/ml, 19 of these mAbs have an epitope on the
222 RBD and all of these block ACE2/RBD interaction, whilst mAb 159 binds the NTD. We used
223 biolayer interferometry (BLI) to measure the affinity of the RBD-binding antibodies and found
224 that compared to Victoria (SARS-CoV-2/human/AUS/VIC01/2020), an early isolate of SARS-
225 CoV-2, which has a single change S247R in S compared to the Wuhan strain (Seemann et al.,
226 2020; Caly et al., 2020) monoclonal antibody binding was significantly impacted with a
227 number showing complete knock-out of activity (**Figure 2I**). The results with P.1 showed a
228 greater impact compared to B.1.1.7 but similar to B.1.351 (Zhou et al., 2021), this is expected

229 since both contain mutation of the same 3 residues in the RBD, only differing at position 417,
230 K417N in B.1.351 and K417T in P.1. The localization of the impact on binding is shown in
231 **Figure 2J** and reflects direct interaction with mutated residues. Of note is mAb 222 which
232 maintains binding potency across all variants despite adjacency to mutated residues, as
233 discussed below.
234
235 *Neutralization of P.1 by potent human monoclonal antibodies*
236 Using the same set of 20 potent antibodies neutralization was measured by a focus reduction
237 neutralization test (FRNT) and compared with neutralization of Victoria and variants B.1.1.7
238 and B.1.351. Compared to Victoria neutralization by the monoclonal antibodies was
239 significantly impacted by P.1, with 12/20 showing >10-fold reduction in FRNT50 titre and a
240 number showing complete knock out of activity (**Figure 3A Table S2**). The results with P.1
241 showed a greater impact compared to B.1.1.7 but were as expected similar to those with
242 B.1.351 (Zhou et al., 2021). There is good correlation between the negative impact on
243 neutralization and on RBD-affinity (**Figure 2J**).
244
245 *Reduced neutralization of P.1 by monoclonal antibodies being developed for clinical use.*
246 A number of potent neutralizing antibodies are being developed for clinical use either
247 therapeutically of prophylactically (Ku et al., 2021;Baum et al., 2020;Kemp et al., 2021). We
248 performed neutralization assays against P.1 using antibodies S309 Vir (Pinto et al., 2020),
249 AZD8895, AZD1061 and AZ7442 (a combination of AZD8895 and AZD1061) AstraZeneca,
250 REGN10987 and REGN10933 Regeneron, LY-CoV555 and LY-CoV16 Lilly and ADG10,
251 ADG20 and ADG30 from Adagio (**Figure 3B**). The affinity of binding to P.1 RBD was also
252 investigated by BLI for the Regeneron and AstraZeneca antibodies and the results (**Figure 2I**)
253 parallel closely the neutralization results. Neutralization of both Lilly antibodies was severely

254 impacted with LY-CoV16 and LY-CoV555 showing almost complete loss of neutralization of
255 P.1 and B.1.351 while LY-CoV16 also showed marked reduction in neutralization of B.1.1.7.
256 There was also escape from neutralization of P.1 by REGN10933 and a modest reduction in
257 neutralization of P.1 by AZD8895, while AZD1061 and AZD 7442 showed equal
258 neutralization of all SARS-CoV-2 variants. The three Adagio antibodies neutralized all variants
259 with all reaching a plateau at 100% neutralization and interestingly, ADG30 showed a slight
260 increase of neutralization of P.1. S309 Vir was largely unaffected although for several viruses,
261 including P.1, the antibody failed to completely neutralize, conceivably reflecting incomplete
262 glycosylation at N343, since the sugar interaction is key to binding of this antibody N343 (Pinto
263 et al., 2020). The escape from REGN10933 and LY-CoV555 mirrors that of other potent
264 antibodies (including 316 and 384 in our set) which make strong interactions with residues
265 484-486 and are severely compromised by the marked change E484K, whereas LY-CoV016,
266 an IGHV3-53 mAb, is affected by changes at 417 and 501. The abrogation of the Lilly Ly-
267 CoV-16 and LyCoV-555 antibodies reflects the observation of Starr et al. (Starr et al.,
268 2021)(Greaney et al., 2021) that LY-CoV555 is sensitive to mutation at residue 384 and LY-
269 CoV16 is sensitive to changes at 417.
270
271 *Reduced neutralization by an NTD-binding antibody*
272 The neutralization titre of NTD-binding mAb159, was 133-fold reduced on P.1 compared to
273 Victoria with only 64% neutralization at 10μg/ml (**Figures 3A**). Although P.1 does not harbor
274 deletions in the NTD like B.1.1.7 (Δ69−70, Δ144) or B.1.351 (Δ242−244), it is clear that the 6
275 NTD mutations in P.1 (L18F, T20N, P26S, D138Y, R190S) disrupt the epitope for mAb159
276 (**Figure 4A**) (Dejnirattisai et al., 2021;Supasa et al., 2021). It is possible that the failure of this
277 antibody to achieve complete neutralization could be due to partial glycosylation at residue 20,
278 which is some 16 Å from bound Fab 159, however the L18F mutation is even closer and likely

279 to diminish affinity (**Figure 4A**). Since it has been proposed that there is a single supersite for
280 potent NTD binding antibodies we would expect the binding of many of these to be affected
281 (Cerutti et al., 2021).
282
283 *Reduced neutralization by VH3-53 public antibodies*
284 Five of the potent monoclonal antibodies used in this study (150, 158, 175, 222 and 269),
285 belong to the VH3-53 family and a further 2 (out of 5 of this family) belong to the almost
286 identical VH3-66, and the following discussion applies also to these antibodies. The binding
287 sites for these have been described (Dejnirattisai et al., 2021). The large majority of these
288 antibodies attach to the RBD in a very similar fashion. These motifs recur widely, VH3-53 are
289 the most prevalent deposited sequences and structures for SARS-CoV-2 neutralizing
290 antibodies. Their engagement with the RBD is dictated by CDR-H1 and CDR-H2 whilst the
291 CDR-H3 is characteristically short and makes rather few interactions (Yuan et al., 2020; Barnes
292 et al., 2020;Dejnirattisai et al., 2021). We have previously solved the structures of mAbs 150,
293 158 and 269 (**Figure 4B**) which show that whilst there are no contacts with residue 484, there
294 are interactions of CDR-H3 with K417 and CDR-L1 with N501, meaning that binding and
295 neutralization by VH3-53 antibodies would be predicted to be compromised by the N501Y
296 change in variant viruses B.1.1.7, B.1.351 and P.1, whilst the additional change at 417 in P.1
297 (K417T) and B.1.351 (K417N) might be expected to have an additive effect (Dejnirattisai et
298 al., 2021).
299
300 In practice, changes in the light chain and CDR-H3 between members of this family mean that
301 the story is more complex. Thus, neutralization of P.1 by 175 and 158 is severely impacted and
302 neutralization of P.1 by 269 is almost completely lost. However, for 150 P.1 neutralization is

303 less compromised than for B.1.351 (Zhou et al., 2021), whilst for 222 neutralization is
304 completely unaffected by the changes in P.1 and indeed all variants (**Figure 3A**).
305
306 We measured the affinity of 222 for both P.1 (KD = 1.92±0.01 nM) and Wuhan RBD (KD =
307 1.36±0.08 nM) showing no reduction in the strength of interaction despite the changes
308 occurring in the putative binding site for P.1 (**Table S2**).
309
310 To understand how 222 is able to still neutralize P.1 we solved the crystal structures of six
311 ternary complexes of 222 in complex with the RBDs for (i) the original virus, and bearing
312 mutations (ii) K417N; (iii) K417T; (iv) N501Y; the 417, 484 and 501 changes characteristic
313 of B.1.351 (v) and P.1 (vi). All crystals also contained a further Fab, EY6A as a crystallization
314 chaperone (Zhou et al., 2020), were isomorphous and the resolution of the structures ranged
315 from 1.95 to 2.67 Å, **Figure 4C,D**, Methods, **Table S1**. As expected, the structures are highly
316 similar with the binding pose of 222 being essentially identical in all structures (pairwise
317 RMSD in Cα atoms between pairs of structures are ~0.2-0.3 Å for all residues in the RBD and
318 Fv region of mAb 222, **Figure 4D**).
319
320 In the original virus residue 417 makes a weak salt bridge interaction with heavy chain CDR3
321 residue E99. Mutation to either Asn or Thr abolishes this and there is little direct interaction,
322 although there are weak (~3.5 Å) contacts to heavy chain Y52 and light chain Y92 (**Figure**
323 **4E**). However, a buffer molecule/ion rearranges to form bridging interactions and this may
324 mitigate the loss of the salt bridge, in addition the original salt bridge is weak and its
325 contribution to binding may be offset by the loss of entropy in the lysine sidechain. We note
326 that CDR-H3 of 222, at 13 residues is slightly longer than found in the majority of potent VH3-
327 53 antibodies, however this seems unlikely to be responsible for the resilience of 222, rather it

328 seems that there is little binding energy in general from the CDR3-H3, since most of the binding
329 energy contribution of the heavy chain comes from CDR-H1 and CDR-H2 which do not
330 interact with RBD residue 417, meaning that many VH3-53 antibodies are likely to be resilient
331 to the common N/T mutations (**Figure 4B**).
332
333 Residue 501 makes contact with CDR-L1 of mAb 222 (**Figure 4D,F**), however the interaction,
334 with P30 is probably slightly strengthened by the N501Y mutation which provides a stacking
335 interaction with the proline, conferring resilience. This is in contrast to the situation with most
336 other VH3.53 antibodies where direct contacts confer susceptibility to escape by mutation to
337 Tyr (**Figures 2I,J and 3A**) (Supasa et al., 2021;Zhou et al., 2021).
338
339 *The 222 light chain can rescue neutralization by other VH3-53 mAbs*
340 Reasoning that the relative robustness of mAb 222 to common variants (P.1, B.1.1.7 and
341 B.1.351) compared to other VH3-53 antibodies stems from the choice of light chain we
342 modelled the 222LC with the heavy chains of other VH3-53 antibodies to see if they might be
343 compatible **(Figure 4G)**. The result was striking, it appeared that there would likely be no
344 serious steric clashes. This contrasted with the numerous clashes seen when we docked the
345 light chains of other VH3-53 antibodies onto the heavy chain of 222 (**Figure 4G,H**). This
346 suggests that the 222 light chain might be an almost universal light chain for these 3-53
347 antibodies and could confer resilience to P.1, B.1.1.7 and B.1.351 variants. This led us to create
348 chimeric antibodies containing the 222LC combined with the HC of the other VH3-53 mAbs
349 150, 158, 175 and 269. In all cases, chimeric antibodies expressed well and we performed
350 neutralization assays against Victoria, B.1.1.7, B.1.351 and P.1 viruses **(Figure 5)**. For B.1.1.7
351 neutralization of 150HC/222LC, 158HC/222LC and 269HC/222LC was restored to near the
352 level seen on Victoria, whilst 175HC/222LC could not fully neutralize B.1.1.7. For B.1.351

353 and P.1 the activity of mAbs 150 and 158 was restored in chimeras containing the 222LC, with
354 the 150HC/222LC showing 50-fold greater potency against B.1.351 (7ng vs 350 ng/ml) and
355 13-fold greater potency against P.1 (3ng vs 40 ng/ml) than native 150. With an FRNT50 of
356 3ng/ml 150HC/222LC was the most potent antibody tested against P.1.
357
358 *Neutralization of P.1 by convalescent plasma*
359 We collected convalescent plasma samples from a cohort of volunteers who had suffered from
360 SARS-CoV-2 infection evidenced by a positive diagnostic PCR. Samples were collected
361 during the convalescent phase, 4-9 weeks following infection, all samples were taken during
362 the first wave of infection in the UK, prior June 2020 and well before the emergence of the
363 B.1.1.7 variant. We have also collected plasma from volunteers recently infected with B.1.1.7
364 as demonstrated by viral sequencing or S gene drop out from the diagnostic PCR (Dejnirattisai
365 et al., 2021;Supasa et al., 2021).
366
367 Neutralization of P.1 was assessed by FRNT on 34 convalescent samples **(Figure 6A Table**
368 **S3A)**. P.1 neutralization curves are displayed alongside neutralization curves for Victoria,
369 together with B.1.1.7 and B.1.351. P.1 geometric mean neutralization titres were reduced 3.1-
370 fold compared to Victoria ($p < 0.0001$). This reduction was similar to B.1.1.7 (2.9-fold) and
371 considerably less than B.1.351 (13.3-fold) **(Figure 6C)**. When using plasma from individuals
372 infected with B.1.1.7 we saw only modest (1.8-fold $p=0.0039$) reductions in neutralization
373 comparing P.1 with Victoria **(Figure 6B and D Table S3B)**.
374
375 *Neutralization of P.1 by vaccine serum*
376 We next performed neutralization assays using serum collected from individuals who had
377 received either the BNT162b2 Pfizer-BioNTech or ChAdOx1 nCoV-19 Oxford-AstraZeneca

378 vaccine **Figure 7** (Supasa et al., 2021;Zhou et al., 2021). For the Pfizer BioNTech vaccine
379 serum was collected 4-14 days following the second dose of vaccine administered three weeks
380 after the first dose (n=25). For the Oxford-AstraZeneca vaccine serum was taken 14 or 28 days
381 following the second dose which was administered 8-14 weeks following the first dose (N=25).
382 Geometric mean neutralization titres against P.1 were reduced 2.6-fold ($p<0.0001$) relative to
383 the Victoria virus for the Pfizer-BioNTech vaccine serum **Figure 7A,C** and 2.9-fold
384 ($P<0.0001$) for the Oxford-AstraZeneca vaccine **Figure 7B,D Table S4.**
385
386 Neutralization titres against P.1 were similar to those against B.1.1.7 and only a minority of
387 samples failed to reach 100% neutralization at 1:20 dilution of serum, considerably better than
388 neutralization of B.1.351, where titres were reduced 7.6-fold and 9-fold for the BNT162b2
389 Pfizer and ChAdOx1 nCoV-19 AstraZeneca vaccines respectively.
390
391 **Discussion**
392
393 Large scale viral sequencing programmes have uncovered a spectrum of mutations containing
394 changes at many locations in the SARS-CoV-2 genome in correspondence with the concept of
395 viral quasispecies (Domingo and Perales, 2019). Mutations in S are of particular concern as S,
396 through the RBD, directs cellular tropism and in addition is the target for the neutralizing
397 antibody response. Mutations in S could therefore enhance viral fitness by increasing affinity
398 to ACE2 or provide escape from the antibody response induced by natural infection or
399 vaccination.
400
401 P.1 contains 12 individual changes spread throughout S with three changes in the RBD. In this
402 paper we demonstrate an increase in affinity of interaction for P.1 RBD with ACE2 to an

403 equivalent degree as that observed for B.1.351 with binding somewhat tighter than for B.1.1.7.
404 It seems conceivable that this increase in receptor affinity may drive increased virus
405 transmissibility, allowing the three variants to become dominant strains in the regions where
406 they emerged (Zhou et al., 2021;Supasa et al., 2021).
407
408 The ACE2 interacting surface of RBD is a small 25 amino acid patch at the apex of S and is
409 under extreme selection pressure as it not only mediates interaction with the cellular receptor
410 but is also the site of binding for a major class of neutralizing antibodies that block the
411 interaction of ACE2 with the RBD (Zost et al., 2020;Kreye et al., 2020;Wu et al., 2020;Yuan
412 et al., 2020). (Dejnirattisai et al., 2021). Recently, two elegant unbiased approaches have been
413 used to assess the influence of mutation on the ACE2/RBD binding affinity or the ability of
414 RBD mutations to evade the polyclonal antibody response. Firstly, a yeast display approach
415 was used to generate RBD mutants with enhanced ACE2 binding. Amongst a number of
416 mutations selected were the very same positions found in the recent variants of concern, namely
417 E484K and N501Y, and less frequently changes at residue 417 were also observed (Zahradník
418 et al., 2021). Multiple rounds of selection led to the emergence of mutant RBDs with 600-fold
419 higher affinity to ACE2, in the low picomolar range. In a second approach, polyclonal anti-
420 SARS-CoV-2 serum was used to select mutant RBD from a yeast display library which showed
421 reduced antibody binding (Greaney et al., 2021). This approach led to the identification of a
422 number of potential antibody escape mutants, amongst them E484 which is likely responsible
423 for a proportion of the escape from antibody neutralization we describe for P.1.
424
425 What is driving the emergence of the new strains is difficult to determine, the emergence of
426 B.1.1.7 occurred on the background of relatively low population immunity and may have been
427 primarily driven by increased transmissibility. The emergence of B.1.351 occurred on the

428 background of around 30% seropositivity in South Africa and P.1 on the background of an
429 estimated 75% seropositivity in Manaus Brazil (Faria et al., 2021). It seems possible that
430 selection of P.1 and B.1.351 may have been in part driven by immune escape, however until
431 methods are developed to screen at a population level for the frequency of reinfection, it is not
432 possible to determine this, especially as reinfection may lead to more mild or asymptomatic
433 disease.
434
435 Because P.1 and B.1.351 contain very similar changes in the RBD it might be assumed that
436 neutralization of both would be similarly affected. This was indeed the case for neutralization
437 by monoclonal antibodies directed at the RBD, where there was substantial escape from many
438 antibodies in our panel or from antibodies being developed for clinical use. However,
439 neutralization of P.1 was not compromised as severely as neutralization of B.1.351, when using
440 convalescent or vaccine serum induced by earlier SARS-CoV-2 strains(Zhou et al., 2021).
441 Using convalescent serum B.1.351 showed 13-fold reduction in neutralization compared to
442 Victoria whilst P.1 was only reduced 3.1-fold, comparable to the reduction seen with B.1.1.7,
443 which only harbours the single N501Y change in the RBD (Zhou et al., 2021;Supasa et al.,
444 2021). Similarly, neutralization of P.1 by vaccine serum was less impacted than neutralization
445 of B.1.351 meaning that vaccination with Wuhan S will likely provide some protection against
446 P.1. There is now clinical evidence that the ChAdOx1 nCoV-19 Oxford-AstraZeneca and
447 NVX-CoV2373 Novavax vaccines provide protection from B.1.1.7 (Emary et al.,
448 2021;Mahase, 2021). For B.1.351 both the Novavax
449 (https://www.webmd.com/vaccines/covid-19-vaccine/news/20210131/vaccine-not-as-
450 effective-against-south-african-variant) and Janssen vaccine
451 (https://www.reuters.com/article/us-health-coronavirus-vaccines-johnson-j-
452 idUSKBN29Z0F0) saw a marked decrease in efficacy against B.1.351, but still showed >50%

453 protection against moderate and severe disease, whilst in a Phase II trial, ChAdOx1 nCoV-19
454 efficacy against mild to moderate disease caused by B.1.351 was 10.4% (95% CI: –76.8; 43.8),
455 but efficacy against severe disease could not be assessed in this study (Madhi et al., 2021).
456
457 The reason for the differences in neutralization of B.1.351 and P.1 by immune serum are not
458 immediately clear, but presumably reflect the difference in the mutations introduced outside
459 the RBD. In addition to our mAb 159 a number of potent neutralizing mAbs have been reported
460 that map to the NTD (Cerutti et al., 2021), and this domain has multiple mutations in all three
461 major variant strains: B.1.1.7 has two deletions, B.1.351 has a deletion and four substitutions
462 and P.1 has 6 amino acid substitutions, including the creation of two N-linked glycan sequons
463 (**Figure 1 A-C**). Comparison of neutralization of pseudoviruses expressing only the three RBD
464 mutations (K417N E484K N501Y) of B.1.351 with pseudovirus expressing the full suite of
465 mutations in B.1.351 spike show that the non-RBD changes substantially increase escape from
466 neutralization (Wibmer et al., 2021;Dejnirattisai et al., 2021;Wang et al., 2021). The changes
467 in the NTD of the major variants are far less consistent than those found in the RBD, and there
468 are no strong trends in electrostatic properties (**Figure 1A-C**). It therefore remains unclear what
469 the drivers are for these changes, although one or more of immune escape, co-receptor binding,
470 and modulation of RBD dynamics affecting presentation of the receptor binding site are
471 plausible. Nonetheless, it seems likely that these changes are largely responsible for the non-
472 RBD component of neutralization variation between strains.
473
474 A number of public antibody responses have been reported for SARS-CoV-2, principal
475 amongst these being VH3-53/VH3-66 and VH1-58 (VH3-30 is also found but the antibodies
476 are not potent neutralizers) (Yuan et al., 2020;Barnes et al., 2020; Dejnirattisai et al., 2021).
477 We have previously shown that mixing heavy and light chains from antibodies within VH1-58

478 can increase the neutralization titre by 20-fold from the parent antibodies (chimera of 253HC
479 with 55LC or 165LC) (Dejnirattisai et al., 2021). Here we have shown that chimeras created
480 amongst the VH3-53 antibodies using the 222LC are able to confer broad neutralization to
481 antibodies which have reduced neutralization capacity against the viral variants. Furthermore,
482 the chimera of 150HC with 222LC achieved 13 and 3-fold increases in neutralization titre
483 compared to the parental 150 and 222 mAb respectively. Creation of such antibody chimeras
484 amongst other anti-SARS-CoV2 antibodies may similarly lead to the discovery of more
485 antibodies with enhanced activity. This also suggests that highly effective natural responses
486 against all three variants, and common cross-protective responses, will be found.
487
488 The recent emergence of a number of variants of concern has led to efforts to design new
489 vaccines which will be able to protect against the viral variants. Exactly which variants or
490 sequences should be selected is difficult to determine in what is likely to be an evolving
491 situation, as vaccine induced herd immunity increases the selection pressure for immune
492 escape. Based on the results reported here the South African B.1.351 is the variant of greatest
493 concern giving the largest reductions in neutralization titres and evidence of complete failure
494 to neutralize in some cases and we believe developing vaccine constructs to B.1.351 to be the
495 greatest priority.
496
497 In summary, we demonstrate that P.1 can escape neutralization by a number of monoclonal
498 antibodies including some being developed for prophylactic or therapeutic use, while other
499 antibodies with epitopes away from the mutated RBD residues retain broad neutralization.
500 Thus S309/AZD1061/REGN10987/ADG10/ADG20/ADG30 showed little to no reduction
501 (<4-fold) in neutralization activity across the three variants, consistent with their previously
502 described broadly neutralizing activities across clade I sarbecoviruses.

503

504 In contrast to B.1.351, neutralization of P.1 does not show such a substantial reduction by
505 polyclonal serum induced by natural infection or vaccination and there is no evidence of
506 widespread escape. Despite the reduction in neutralization titres it is hoped that immunization
507 with vaccines designed against parent/ancestral strains will provide protection from P.1.

508

509 **Limitations of the study**

510

511 The in vitro FRNT assays we report here do not measure the effect of complement or antibody
512 dependent cell mediated cytotoxicity which may enhance neutralization in vivo. The role that
513 T cells play in immunity to SARS-CoV-2 and in particular protection from severe disease is
514 unknown and worthy of investigation, but recent findings suggest that CD4 and CD8 T cell
515 responses raised to ancestral strains are minimally impacted by the variants (Alison Tarke et
516 al., 2021;Skelly et al., 2021). It will be interesting to determine the directionality of
517 neutralization between the different variant viruses and naturally acquired antibody responses
518 to them. For instance, there is some suggestion in this report that plasma induced by B.1.1.7 is
519 better able to neutralize B.1.351 and P.1. Measuring neutralization of viral variants by B.1.351
520 and P.1 serum will give a better idea of cross protection against the other strains.

521

522 **Acknowledgements**

523 This work was supported by the Chinese Academy of Medical Sciences (CAMS) Innovation
524 Fund for Medical Science (CIFMS), China (grant number: 2018-I2M-2-002) to D.I.S. and
525 G.R.S. H.M.E.D. and J.Ren are supported by the Wellcome Trust (101122/Z/13/Z), Y.Z. by
526 Cancer Research UK (C375/A17721), TAB and RJGH by the UKRI MRC (MR/S007555/1),
527 D.I.S. and E.E.F. by the UKRI MRC (MR/N00065X/1). D.I.S. is a Jenner Investigator. The

528 National Institute for Health Research Biomedical Research Centre Funding Scheme supports
529 G.R.S. We are also grateful for a Fast Grant from Fast Grants, Mercatus Center to support the
530 isolation of human monoclonal antibodies to SARS-CoV-2 and Schmidt Futures for support of
531 this work. G.R.S. is also supported as a Wellcome Trust Senior Investigator (grant
532 095541/A/11/Z). This is a contribution from the UK Instruct-ERIC Centre. The Wellcome
533 Centre for Human Genetics is supported by the Wellcome Trust (grant 090532/Z/09/Z). Virus
534 used for the neutralisation assays was isolated by Julian Druce, Doherty Centre, Melbourne,
535 Australia. Chanice Knight, Emily Chiplin, Ross Fothergill and Liz Penn contributed to assays.
536 We acknowledge Diamond Light Source for time on Beamline I03 under Proposal lb27009 for
537 COVID-19 Rapid Access. Huge thanks to the teams, especially at the Diamond Light Source
538 and Department of Structural Biology, Oxford University that have enabled work to continue
539 during the pandemic. The computational aspects of this research were supported by the
540 Wellcome Trust Core Award Grant Number 203141/Z/16/Z and the NIHR Oxford BRC. The
541 Oxford Vaccine work was supported by UK Research and Innovation, Coalition for Epidemic
542 Preparedness Innovations, National Institute for Health Research (NIHR), NIHR Oxford
543 Biomedical Research Centre, Thames Valley and South Midland's NIHR Clinical Research
544 Network. We thank the Oxford Protective T-cell Immunology for COVID-19 (OPTIC) Clinical
545 team for participant sample collection and the Oxford Immunology Network Covid-19
546 Response T cell Consortium for laboratory support. We acknowledge the rapid sharing of
547 Victoria, B.1.1.7 and B.1.351 which was isolated by scientists within the National Infection
548 Service at PHE Porton Down. We thank The Secretariat of National Surveillance, Ministry of
549 Health Brazil for assistance in obtaining P.1 samples. This work was supported by the UK
550 Department of Health and Social Care as part of the PITCH (Protective Immunity from T cells
551 to Covid-19 in Health workers) Consortium, the UK Coronavirus Immunology Consortium
552 (UK-CIC) and the Huo Family Foundation. EB and PK are NIHR Senior Investigators and PK

is funded by WT109965MA and NIH (U19 I082360). DS is an NIHR Academic Clinical Fellow. The views expressed in this article are those of the authors and not necessarily those of the National Health Service (NHS), the Department of Health and Social Care (DHSC), the National Institutes for Health Research (NIHR), the Medical Research Council (MRC) or Public Health, England.

Author Information

These authors contributed equally: WD, DZ, PS, CL, AJM.

Contributions

Contributions

D.Z. performed BLI interaction analyses. D.Z., J.R., N.G.P., M.A.W. and D.R.H. prepared the crystals, enabled and performed X-ray data collection. J.R., E.E.F., H.M.E.D. and D.I.S. analysed the structural results. G.R.S., J.M., P.S., Y.Z., D.Z., G.C.P, B.W., R.N., A.T., J.S-C., C.L-C. and C.L. prepared the Spike constructs, RBDs, ACE2 and antibodies and, W.D. and P.S. performed neutralization assays. D.C. provided materials. H.M.G. wrote MABSCAPE and performed mapping and cluster analysis, including sequence analyses. S.A.C.C., P. G. N., V.N., F. N., C. F. C., A.J.M., E.B., S.J.D., D.S., C.D., R.L., T.D., A.J.P., J.C.K., P.K., M.W.C., T.L., S.B., A.F., M.B., S.B-R., E.C. and S.G. assisted with patient samples and vaccine trials. E.B., M.C., S.J.D., P.K. and D.S. conceived the study of vaccinated healthcare workers and oversaw the OPTIC Healthcare Worker study and sample collection/processing. G.R.S. and D.I.S. conceived the study and wrote the initial manuscript draft with other authors providing editorial comments. R.J.G.H. and T.A.B. contributed to study design. All authors read and approved the manuscript.

578 **Competing Financial Interests**

579 GRS sits on the GSK Vaccines Scientific Advisory Board. Oxford University holds intellectual
580 property related to the Oxford-AstraZeneca vaccine. AJP is Chair of UK Dept. Health and
581 Social Care's (DHSC) Joint Committee on Vaccination & Immunisation (JCVI) but does not
582 participate in the JCVI COVID19 committee, and is a member of the WHO's SAGE. The views
583 expressed in this article do not necessarily represent the views of DHSC, JCVI, or WHO. The
584 University of Oxford has entered into a partnership with AstraZeneca on coronavirus vaccine
585 development.
586 The University of Oxford has protected intellectual property disclosed in this publication.
587
588
589 **Figure Legends**
590
591 **Figure 1. Mutational landscape of P.1.** Schematic showing the locations of amino acid
592 substitutions in (A) P.1, (B) B.1.351 and (C) B.1.1.7 relative to the Wuhan SARS-CoV-2
593 sequence. Under the structural cartoon is a linear representation of S with changes marked on.
594 Where there is a charge change introduced by mutations the change is coloured (red if the
595 change makes the mutant more acidic/less basic, blue more basic/less acidic). (D) Depiction of
596 the RBD as a grey surface with the location of the three mutations K417T, E484K and N501Y
597 (magenta) the ACE2 binding surface of RBD is coloured green. (E) locations of N-linked
598 glycan (red spheres) on the spike trimer shown in a pale blue surface representation, the two
599 new sequons found in P.1 are marked blue.
600
601 **Figure 2. Comparison of WT RBD/ACE2 and P.1 RBD/ACE2 complexes.** (A)
602 Comparison of P.1 RBD/ACE2 (grey and salmon) with WT RBD/ACE2 (blue and cyan)

603 (PDB ID 6LZG) by overlapping the RBDs. The mutations in the P.1 RBD are shown as
604 sticks. (B), (C) Open book view of electrostatic surface of the WT RBD/ACE2 complex, and
605 (C), (D) of the P.1 RBD/ACE2 complex. Note the charge difference between the WT and the
606 mutant RBDs. The charge range displayed is ±5 kJ/mol. (E) The K417 of the WT RBD forms
607 a salt bridge with D30 of ACE2. (F) and (G) Effect of E484K mutation on the electrostatic
608 surface (H) Y501 of the P.1 RBD makes a stacking interaction with Y41 of ACE2. (H) K_D of
609 RBD/mAb interaction measured by BLI for RBDs of Victoria, B.1.1.7, P.1 and B.1.351 (left
610 to right) (I) BLI data mapped onto the RBD using the method described (Dejnirattisai *et al.*,
611 2021). Front and back views of the RBD are shown. In the left pair the spheres represent the
612 antibody binding sites coloured according to the ratio (K_DP.1/K_DWuhan). For white the ratio
613 is 1, for red it is <0.1 (i.e. at least 10-fold reduction) black dots refer to mapped antibodies
614 not included in this analysis, dark green RBD ACE2 binding surface, yellow mutated K417T,
615 E484K, N501Y. For the right pair atoms are coloured according to the ratio of neutralisation
616 titres (IC_{50}B.1.351/IC_{50}Victoria), for white the ratio is 1, for red it is <0.01 (i.e. at least 100-
617 fold reduction). Note the strong agreement between K_D and IC_{50}. 269 is very strongly
618 affected and is close to the IGHV3-53 and IGHV3-66 antibodies (*e.g.* 222).
619
620 **Figure 3. Neutralization of P.1 by monoclonal antibodies.** (A) Neutralization of P.1 by a
621 panel of 20 potent human monoclonal antibodies. Neutralization was measured by FRNT,
622 curves for P.1 are superimposed onto curves for Victoria, B.1.1.7 and B.1.351 as previously
623 reported (Supasa et al., 2021;Zhou et al., 2021). FRNT50 titres are reported in Table S2
624 Neutralization curves for monoclonal antibodies in different stages of development for
625 commercial use. (B) Shows equivalent plots for the Vir, Regeneron, AstraZeneca, Lilly and
626 Adagio antibodies therapeutic antibodies.
627

628 **Figure 4. Structures of Fab 222 in complex with P.1 RBD.** (A) Ribbon depiction of Fab
629 159/NTD complex with P1 mutations in the NTD highlighted as cyan spheres. (B) Front and
630 back surfaces of the RBD bound to a typical VH3-53. P1 mutations in the RBD are highlighted
631 in dark green and labelled. In this group, monoclonal antibody 222 has a slightly longer CDR3.
632 Sequences of VH3-53 CDR1-3 heavy and light chains are also shown. (C) Crystal structure of
633 P1 RBD, 222 Fab and EY6A Fab (Zhou et al., 2020). (D) Close up of 222 CDRs interacting
634 with the RBD (grey) mutations are highlighted in yellow on the green ACE2 interface. (E)
635 K417 interactions with Fab 222 (F) N501 interactions with Fab 222. (G), (H) Fab 222 chimera
636 models.
637
638 **Figure 5. Neutralization curves of VH3-53 chimeric antibodies.** Neutralization curves of
639 Victoria, B.1.1.7, B.1.351 and P.1. Left hand column; neutralization curves using the native
640 antibodies 222, 150, 158, 175 and 269. Right hand column; neutralization curves for chimeric
641 antibodies, the heavy chains of 150, 158, 175 and 269 are combined with the light chain of
642 222, native 222 is used as the control. FRNT50 titres are given in Table S2.
643
644 **Figure 6 Neutralization of P.1 by convalescent plasma.** Plasma (n=34) was collected from
645 volunteers 4-9 weeks following SARS-CoV-2 infection, all samples were collected before June
646 2020 and therefore represent infection before the emergence of B.1.1.7 in the UK. (A)
647 Neutralization of P.1 was measured by FRNT, comparison is made with neutralization curves
648 for Victoria, B.1.1.7 and B.1.351 that we have previously generated (Zhou et al., 2021;Supasa
649 et al., 2021). (B) Neutralization of P.1 by plasma taken from volunteers who had suffered
650 infection with B.1.1.7 as evidenced by sequencing or S-gene drop out by diagnostic PCR.
651 Samples were taken at varying times following infection. (C-D) Comparison of FRNT50 titres
652 between Victoria and P.1, data for B.1.1.7 and B.1.351 are included for comparison and, the

653 Wilcoxon matched-pairs signed rank test was used for the analysis and two-tailed P values
654 were calculated, geometric mean values are indicated above each column.
655
656 **Figure 7 Neutralization of P.1 by vaccine serum.** (A) Pfizer vaccine, serum (n=25) was taken
657 7-17 days following the second dose of the Pfizer-BioNTech vaccine. FRNT titration curves
658 are shown with Victoria, B.1.1.7 and B.1.351 as comparison (Supasa et al., 2021;Zhou et al.,
659 2021). (B) AstraZenca vaccine, serum was taken 14 or 28 days following the second dose of
660 the Oxford-AstraZeneca vaccine (n=25). (C-D) Comparison of FRNT50 titres for individual
661 samples for the Pfizer and AstraZeneca vaccine between Victoria, B.1.1.7, B.1.351 and P.1,
662 the Wilcoxon matched-pairs signed rank test was used for the analysis and two-tailed P values
663 were calculated, geometric mean values are indicated above each column.
664
665 **STAR Methods**
666 **RESOURCE AVAILABILITY**
667 *Lead Contact*
668 Resources, reagents and further information requirement should be forwarded to and will be
669 responded by the Lead Contact, David I Stuart (dave@strubi.ox.ac.uk).
670 *Materials Availability*
671 Reagents generated in this study are available from the Lead Contact with a completed
672 Materials Transfer Agreement.
673 *Data and Code Availability*
674 The coordinates and structure factors of the crystallographic complexes are available from the
675 PDB with accession codes (see Table S1). Mabscape is available from
676 https://github.com/helenginn/mabscape, https://snapcraft.io/mabscape. The data that support
677 the findings of this study are available from the corresponding authors on request.

678

679 **EXPERIMENTAL MODEL AND SUBJECT DETAILS**

680 *Viral stocks*

681 SARS-CoV-2/human/AUS/VIC01/2020 (Caly et al., 2020), SARS-CoV-2/B.1.1.7 and SARS-
682 CoV-2/B.1.351 were provided by Public Health England, P.1 from a throat swab from Brazil
683 were grown in Vero (ATCC CCL-81) cells. Cells were infected with the SARS-CoV-2 virus
684 using an MOI of 0.0001. Virus containing supernatant was harvested at 80% CPE and spun at
685 3000 rpm at 4 °C before storage at -80 °C. Viral titres were determined by a focus-forming
686 assay on Vero cells. Victoria passage 5, B.1.1.7 passage 2 and B.1.351 passage 4 stocks were
687 sequenced to verify that they contained the expected spike protein sequence and no changes to
688 the furin cleavage sites. The P.1 virus used in these studies contained the following mutations:
689 L18F, T20N, P26S, D138Y, R190S, K417T, E464K, N501Y, D614G, H655Y, T1027I,
690 V1176F. Passage 1 P.1 virus was sequence confirmed and contained no changes to the furin
691 cleavage site.

692 *Bacterial Strains and Cell Culture*

693 Vero (ATCC CCL-81) cells were cultured at 37 °C in Dulbecco's Modified Eagle medium
694 (DMEM) high glucose (Sigma-Aldrich) supplemented with 10% fetal bovine serum (FBS), 2
695 mM GlutaMAX (Gibco, 35050061) and 100 U/ml of penicillin–streptomycin. Human mAbs
696 were expressed in HEK293T cells cultured in UltraDOMA PF Protein-free Medium (Cat# 12-
697 727F, LONZA) at 37 °C with 5% CO_2. *E.coli DH5α* bacteria were used for transformation of
698 plasmids encoding wt and mutated RBD proteins. A single colony was picked and cultured in
699 LB broth with 50 µg mL^{-1} Kanamycin at 37 °C at 200 rpm in a shaker overnight. HEK293T
700 (ATCC CRL-11268) cells were cultured in DMEM high glucose (Sigma-Aldrich)
701 supplemented with 10% FBS, 1% 100X Mem Neaa (Gibco) and 1% 100X L-Glutamine

702 (Gibco) at 37 °C with 5% CO_2. To express RBD, RBD K417T, E484K, N501Y, RBD K417N,
703 RBD K417T, RBD E484K and ACE2, HEK293T cells were cultured in DMEM high glucose
704 (Sigma) supplemented with 2% FBS, 1% 100X Mem Neaa and 1% 100X L-Glutamine at 37
705 °C for transfection.

706 *Participants*

707 Participants were recruited through three studies: Sepsis Immunomics [Oxford REC C,
708 reference:19/SC/0296]), ISARIC/WHO Clinical Characterisation Protocol for Severe
709 Emerging Infections [Oxford REC C, reference 13/SC/0149] and the Gastro-intestinal illness
710 in Oxford: COVID sub study [Sheffield REC, reference: 16/YH/0247]. Diagnosis was
711 confirmed through reporting of symptoms consistent with COVID-19 and a test positive for
712 SARS-CoV-2 using reverse transcriptase polymerase chain reaction (RT-PCR) from an upper
713 respiratory tract (nose/throat) swab tested in accredited laboratories. A blood sample was taken
714 following consent at least 14 days after symptom onset. Clinical information including severity
715 of disease (mild, severe or critical infection according to recommendations from the World
716 Health Organisation) and times between symptom onset and sampling and age of participant
717 was captured for all individuals at the time of sampling.

718

719 P.1 virus from throat swabs. The International Reference Laboratory for Coronavirus at
720 FIOCRUZ (WHO) as part of the national surveillance for coronavirus had the approval of the
721 FIOCRUZ ethical committee (CEP 4.128.241) to continuously receive and analyze samples of
722 COVID-19 suspected cases for virological surveillance. Clinical samples (throat swabs)
723 containing P.1 were shared with Oxford University, UK under the MTA IOC FIOCRUZ 21-
724 02.

725

726

727 *Sera from Pfizer vaccinees*

728 Pfizer vaccine serum was obtained 7-17 days following the second dose of the BNT162b2
729 vaccine. Vaccinees were Health Care Workers, based at Oxford University Hospitals NHS
730 Foundation Trust, not known to have prior infection with SARS-CoV-2 and were enrolled in
731 the OPTIC Study as part of the Oxford Translational Gastrointestinal Unit GI Biobank Study
732 16/YH/0247 [research ethics committee (REC) at Yorkshire & The Humber – Sheffield]. The
733 study was conducted according to the principles of the Declaration of Helsinki (2008) and the
734 International Conference on Harmonization (ICH) Good Clinical Practice (GCP) guidelines.
735 Written informed consent was obtained for all patients enrolled in the study. Each received two
736 doses of COVID-19 mRNA Vaccine BNT162b2, 30 micrograms, administered
737 intramuscularly after dilution as a series of two doses (0.3 mL each) 18-28 days apart. The
738 mean age of vaccines was 43 years (range 25-63), 11 male and 14 female.

739

740 *AstraZeneca-Oxford vaccine study procedures and sample processing*

741 Full details of the randomized controlled trial of ChAdOx1 nCoV-19 (AZD1222), were
742 previously published (PMID: 33220855/PMID: 32702298). These studies were registered at
743 ISRCTN (15281137 and 89951424) and ClinicalTrials.gov (NCT04324606 and
744 NCT04400838). Written informed consent was obtained from all participants, and the trial is
745 being done in accordance with the principles of the Declaration of Helsinki and Good Clinical
746 Practice. The studies were sponsored by the University of Oxford (Oxford, UK) and approval
747 obtained from a national ethics committee (South Central Berkshire Research Ethics
748 Committee, reference 20/SC/0145 and 20/SC/0179) and a regulatory agency in the United
749 Kingdom (the Medicines and Healthcare Products Regulatory Agency). An independent
750 DSMB reviewed all interim safety reports. A copy of the protocols was included in previous
751 publications (PMID: 33220855/PMID: 32702298).

752

753 Data from vaccinated volunteers who received two vaccinations are included in this paper.
754 Vaccine doses were either 5×10^{10} viral particles (standard dose; SD/SD cohort n=21) or half
755 dose as their first dose (low dose) and a standard dose as their second dose (LD/SD cohort
756 n=4). The interval between first and second dose was in the range of 8-14 weeks. Blood
757 samples were collected and serum separated on the day of vaccination and on pre-specified
758 days after vaccination e.g. 14 and 28 days after boost.

759

760

761 **METHOD DETAILS**

762 *Focus Reduction Neutralization Assay (FRNT)*

763 The neutralization potential of Ab was measured using a Focus Reduction Neutralization Test
764 (FRNT), where the reduction in the number of the infected foci is compared to a negative
765 control well without antibody. Briefly, serially diluted Ab or plasma was mixed with SARS-
766 CoV-2 strain Victoria or P.1 and incubated for 1 hr at 37 °C. The mixtures were then transferred
767 to 96-well, cell culture-treated, flat-bottom microplates containing confluent Vero cell
768 monolayers in duplicate and incubated for a further 2 hrs followed by the addition of 1.5%
769 semi-solid carboxymethyl cellulose (CMC) overlay medium to each well to limit virus
770 diffusion. A focus forming assay was then performed by staining Vero cells with human anti-
771 NP mAb (mAb206) followed by peroxidase-conjugated goat anti-human IgG (A0170; Sigma).
772 Finally, the foci (infected cells) approximately 100 per well in the absence of antibodies, were
773 visualized by adding TrueBlue Peroxidase Substrate. Virus-infected cell foci were counted on
774 the classic AID EliSpot reader using **AID ELISpot software.** The percentage of focus
775 reduction was calculated and IC_{50} was determined using the probit program from the SPSS
776 package.

Cloning of ACE2 and RBD proteins

The constructs of EY6A Fab, 222 Fab, ACE2, WT RBD, B.1.1.7 and B.1.351 mutant RBD are the same as previously described (Dejnirattisai et al. 2021, Zhou et al., 2021, Supasa et al., 2021). To clone RBD K417T and RBD K417N, primers of RBD K417T (forward primer 5'-GGGCAGACCGGCACGATCGCCGACTAC-3' and reverse primer 5'-GTAGTCGGCGATCGTGCCGGTCTGCCC) and primers of RBD K417N (forward primer 5'-CAGGGCAGACCGGCAATATCGCCGACTACAATTAC-3' and reverse primer 5'-GTAATTGTAGTCGGCGATATTGCCGGTCTGCCCTG-3') were used separately, together with two primers of pNEO vector (Forward primer 5'- CAGCTCCTGGGCAACGTGCT-3' and reverse primer 5'- CGTAAAAGGAGCAACATAG-3') to do PCR, with the plasmid of WT RBD as the template. To clone P.1 RBD, the construct of B.1.351 RBD was used as the template and the primers of RBD K417T and of pNEO vector mentioned above were used to do PCR. Amplified DNA fragments were digested with restriction enzymes AgeI and KpnI and then ligated with digested pNEO vector. All constructs were verified by sequencing.

Protein production

Protein production was as described in Zhou et al. (Zhou et al., 2020). Briefly, plasmids encoding proteins were transiently expressed in HEK293T (ATCC CRL-11268) cells. The conditioned medium was dialysed and purified with a 5-ml HisTrap nickel column (GE Healthcare) and further polished using a Superdex 75 HiLoad 16/60 gel filtration column (GE Healthcare).

Bio-Layer Interferometry

801 BLI experiments were run on an Octet Red 96e machine (Fortebio). To measure the binding
802 affinity of ACE2 with P.1 RBD and affinities of monoclonal antibodies and ACE2 with native
803 RBD and, RBD K417N, RBD K417T, RBD E484K and RBD K417T E484K N501Y, eachP.1
804 RBD, each RBD was immobilized onto an AR2G biosensor (Fortebio). Monoclonal antibodies
805 (Dejnirattisai et al., 2021) were used as analytes or serial dilutions of ACE2 were used as
806 analytes. All experiments were run at 30 °C. Data were recorded using software Data
807 Acquisition 11.1 (Fortebio) and Data Analysis HT 11.1 (Fortebio) with a 1:1 fitting model used
808 for the analysis.
809
810 *Antibody production*
811 AstraZeneca and Regeneron antibodies were provided by AstraZeneca, Vir, Lilly and Adagio
812 antibodies were provided by Adagio. For the chimeric antibodies heavy and light chains of the
813 indicated antibodies were transiently transfected into 293Y cells and antibody purified purified
814 from supernatant on protein A.
815
816 *Crystallization*
817
818 ACE2 was mixed with P.1 RBD in a 1:1 molar ratio to a final concentration of 12.5 mg ml^{-1}.
819 EY6A Fab, 222 Fab and WT or mutant RBD were mixed in a 1:1:1 molar ratio to a final
820 concentration of 7.0 mg ml^{-1}. All samples were incubated at room temperature for 30 min.
821 Most crystallization experiments was set up with a Cartesian Robot in Crystalquick 96-well X
822 plates (Greiner Bio-One) using the nanoliter sitting-drop vapor-diffusion method, with 100 nl
823 of protein plus 100 nl of reservoir in each drop, as previously described (Water et al., 2003).
824 Crystallization of B.1.1.7 RBD/EY6A/222 complex was set up by hand pipetting, with 500 nl
825 of protein plus 500 nl of reservoir in each drop. Good crystals of EY6A Fab and 222 Fab
826 complexed with WT, K417T, K417N, B.1.1.7, B.1.351 or P.1 RBD were all obtained from

827 Hampton Research PEGRx 2 screen, condition 35, containing 0.15 M Lithium sulfate, 0.1 M
828 Citric acid pH 3.5, 18% w/v PEG 6,000. Crystals of P.1 RBD/ACE2 complex were formed in
829 Hampton Research PEGRx 1 screen, condition 38, containing 0.1 M Imidazole pH 7.0 and
830 20% w/v Polyethylene glycol 6,000.
831
832 *X-ray data collection, structure determination and refinement*
833 Crystals of ternary complexes of WT and mutant RBD/EY6A and 222 Fabs and the P.1.
834 RBD/ACE2 were mounted in loops and dipped in solution containing 25% glycerol and 75%
835 mother liquor for a second before being frozen in liquid nitrogen prior to data collection.
836 Diffraction data were collected at 100 K at beamline I03 of Diamond Light Source, UK. All
837 data (except some of the WT RBD-EY6A-222 Fab complex images) were collected as part of
838 an automated queue system allowing unattended automated data collection
839 (https://www.diamond.ac.uk/Instruments/Mx/I03/I03-Manual/Unattended-Data-
840 Collections.html). Diffraction images of 0.1° rotation were recorded on an Eiger2 XE 16M
841 detector (exposure time of either 0.004 or 0.006 s per image, beam size 80×20 µm, 100% beam
842 transmission and wavelength of 0.9763 Å). Data were indexed, integrated and scaled with the
843 automated data processing program Xia2-dials (Winter, 2010;Winter *et al.*, 2018). A data set
844 of 1080° was collected from 3 positions of a frozen crystal for the WT RBD-EY6A-222 Fab
845 complex. 720° of data was collected for each of the B.1.1.7, P.1 and B.1.351 mutant
846 RBD/EY6A and 222 Fab complexes (each from 2 crystals), and 360° for each of the K417N
847 and K417T RBD with EY6A and 222 Fabs, and ACE2 complexes was collected from a single
848 crystal.
849
850 Structures of WT RBD-EY6A-222 and the P.1 RBD-ACE2 complexes were determined by
851 molecular replacement with PHASER (McCoy et al., 2007) using search models of SARS-

852 CoV-2 RBD-EY6A-H4 (PDB ID 6ZCZ) (Zhou et al., 2020) and RBD-158 (PDB ID, 7BEK)
853 (Dejnirattisai et al., 2021) complexes, and a RBD and ACE2 complex (PDB ID, 6LZG (Wang
854 et al., 2020)), respectively. Model rebuilding with COOT (Emsley and Cowtan, 2004) and
855 refinement with PHENIX (Liebschner et al., 2019) were done for all the structures. The ChCl
856 domains of EY6A are flexible and have poor electron density. Data collection and structure
857 refinement statistics are given in **Table S1**. Structural comparisons used SHP (Stuart et al.,
858 1979), residues forming the RBD/Fab interface were identified with PISA (Krissinel and
859 Henrick, 2007) and figures were prepared with PyMOL (The PyMOL Molecular Graphics
860 System, Version 1.2r3pre, Schrödinger, LLC).

861

862 *Quantification and statistical analysis*

863 Statistical analyses are reported in the results and figure legends. Neutralization was measured
864 by FRNT. The percentage of focus reduction was calculated and IC_{50} was determined using
865 the probit program from the SPSS package. The Wilcoxon matched-pairs signed rank test was
866 used for the analysis and two-tailed P values were calculated and geometric mean values. BLI
867 data were analysed using Data Analysis HT 11.1 (Fortebio) with a 1:1 fitting model.

868

869 References

870 Alison Tarke, A., Sidney, J., Methot, N., Zhang, Y., Dan, J.M., Goodwin, B., Rubiro, P.,
871 Sutherland, A., da Silva Antunes, R., Frazier, A., et al. Negligible impact of SARS-CoV-2
872 variants on CD4 + and CD8 + T cell reactivity in COVID-19 exposed donors and vaccinees.
873 *BioRxiv*. 2021; https://doi.org/10.1101/2021.02.27.433180.
874 Baden, L.R., El Sahly, H.M., Essink, B., Kotloff, K., Frey, S., Novak, R., Diemert, D., Spector,
875 S.A., Rouphael, N., Creech, C.B., et al. Efficacy and Safety of the mRNA-1273 SARS-CoV-2
876 Vaccine. *N. Engl. J. Med*. 2020; **384**: 403-416.

877 Barnes, C.O., West, A.P., Huey-Tubman, K.E., Hoffmann, M.A.G., Sharaf, N.G., Hoffman,
878 P.R., Koranda, N., Gristick, H.B., Gaebler, C., Muecksch, F., et al. Structures of Human
879 Antibodies Bound to SARS-CoV-2 Spike Reveal Common Epitopes and Recurrent Features
880 of Antibodies. *Cell* 2020; **182**: 828–842.
881 Baum, A., Fulton, B.O., Wloga, E., Copin, R., Pascal, K.E., Russo, V., Giordano, S., Lanza,
882 K., Negron, N., Ni, M., et al. Antibody cocktail to SARS-CoV-2 spike protein prevents rapid
883 mutational escape seen with individual antibodies. *Science*. 2020; ***369***: 1014–1018.
884 Caly, L., Druce, J., Roberts, J., Bond, K., Tran, T., Kostecki, R., Yoga, Y., Naughton, W.,
885 Taiaroa, G., Seemann, T., et al. Isolation and rapid sharing of the 2019 novel coronavirus
886 (SARS-CoV-2) from the first patient diagnosed with COVID-19 in Australia. *Med. J. Aust*.
887 2020; ***212***: 459–462.
888 Cerutti, G., Guo, Y., Zhou, T., Gorman, J., Lee, M., Rapp, M., Reddem, E.R., Yu, J., Bahna,
889 F., Bimela, J., et al.. Potent SARS-CoV-2 Neutralizing Antibodies Directed Against Spike N-
890 Terminal Domain Target a Single Supersite. *BioRxiv*. 2021: doi:
891 https://doi.org/10.1101/2021.01.10.426120
892 Dejnirattisai, W., Zhou, D., Ginn, H.M., Duyvesteyn, H.M.E., Supasa, P., Case, J.B., Zhao, Y.,
893 Walter, T.S., Mentzer, A.J., Liu, C., et al. The antigenic anatomy of SARS-CoV-2 receptor
894 binding domain. *Cell* 2021; doi: https://doi.org/10.1016/j.cell.2021.02.032
895 Domingo, E., and Perales, C. Viral quasispecies. *PLoS Genet.* 2019; **15:** e1008271.
896 https://doi.org/10.1371/journal.pgen.1008271
897 Donthu, N., and Gustafsson, A. Effects of COVID-19 on business and research. *J. Bus. Res*.
898 2020; **117**: 284–289.
899 Emary, K.R.W., Golubchik, T., Aley, P.K., Ariani, C. V., Angus, B.J., Bibi, S., Blane, B.,
900 Bonsall, D., Cicconi, P., Charlton, S., et al. Efficacy of ChAdOx1 nCoV-19 (AZD1222)

901 Vaccine Against SARS-CoV-2 VOC 202012/01 (B.1.1.7). *SSRN*. 2021; doi:
902 https://doi.org/10.2139/ssrn.3779160.
903 Emsley, P., and Cowtan, K. Coot: Model-building tools for molecular graphics. *Acta*
904 *Crystallogr. Sect. D Biol. Crystallogr.* 2004; **60**: 2126–2132.
905 Faria, N.R., Claro, I.M., Candido, D., Moyses Franco, L.A., Andrade, P.S., Coletti, T.M., Silva,
906 C.A.M., Sales, F.C., Manuli, E.R., Aguiar, R.S., et al. (2021). Genomic characterisation of an
907 emergent SARS-CoV-2 lineage in Manaus: preliminary findings - SARS-CoV-2 coronavirus /
908 nCoV-2019 Genomic Epidemiology - *Virological*, *virological.org*. Available at:
909 https://virological.org/t/genomic-characterisation-of-an-emergent-sars-cov-2-lineage-in-
910 manaus-preliminary-findings/586 (Accessed: 3 March 2021).
911 Greaney, A.J., Starr, T.N., Gilchuk, P., Zost, S.J., Binshtein, E., Loes, A.N., Hilton, S.K.,
912 Huddleston, J., Eguia, R., Crawford, K.H.D., et al. Complete Mapping of Mutations to the
913 SARS-CoV-2 Spike Receptor-Binding Domain that Escape Antibody Recognition. *Cell Host*
914 *Microbe.* 2021; **29**: 44-57.e9.
915 Hoffmann, M., Kleine-Weber, H., Schroeder, S., Mü, M.A., Drosten, C., and Pö, S. SARS-
916 CoV-2 Cell Entry Depends on ACE2 and TMPRSS2 and Is Blocked by a Clinically Proven
917 Protease Inhibitor. *Cell*. 2020; ***181***: 271-280.e8.
918 Kemp, S.A., Collier, D.A., Datir, R.P., Ferreira, I.A.T.M., Gayed, S., Jahun, A., Hosmillo, M.,
919 Rees-Spear, C., Mlcochova, P., Lumb, I.U., et al. SARS-CoV-2 evolution during treatment of
920 chronic infection. *Nature*. 2021; https://doi.org/10.1038/s41586-021-03291-y
921 Krammer, F. SARS-CoV-2 vaccines in development. *Nature*. 2020; **586**: 516–527.
922 Kreye, J., Reincke, S.M., Kornau, H.C., Sánchez-Sendin, E., Corman, V.M., Liu, H., Yuan,
923 M., Wu, N.C., Zhu, X., Lee, C.C.D., et al. A Therapeutic Non-self-reactive SARS-CoV-2
924 Antibody Protects from Lung Pathology in a COVID-19 Hamster Model. *Cell*. 2020; **183**:
925 1058–1069.

926 Krissinel, E., and Henrick, K. Inference of Macromolecular Assemblies from Crystalline State.
927 *J. Mol. Biol.* 2007; **372**: 774–797.
928 Ku, Z., Xie, X., Davidson, E., Ye, X., Su, H., Menachery, V.D., Li, Y., Yuan, Z., Zhang, X.,
929 Muruato, A.E., et al. Molecular determinants and mechanism for antibody cocktail preventing
930 SARS-CoV-2 escape. *Nat. Commun*. 2021; **12**: 469.
931 Liebschner, D., Afonine, P. V., Baker, M.L., Bunkoczi, G., Chen, V.B., Croll, T.I., Hintze, B.,
932 Hung, L.W., Jain, S., McCoy, A.J., et al. Macromolecular structure determination using X-
933 rays, neutrons and electrons: Recent developments in Phenix. *Acta Crystallogr. Sect. D Struct.*
934 *Biol.* 2019; **75**: 861–877.
935 Lu, R., Zhao, X., Li, J., Niu, P., Yang, B., Wu, H., Wang, W., Song, H., Huang, B., Zhu, N., et
936 al. Genomic characterisation and epidemiology of 2019 novel coronavirus: implications for
937 virus origins and receptor binding. *Lancet.* 2020; ***395***: 565–574.
938 Madhi, S.A., Baillie, V., Cutland, C.L., Voysey, M., Koen, A.L., Fairlie, L., Padayachee, S.D.,
939 Dheda, K., Barnabas, S.L., Bhorat, Q.E., et al. Safety and efficacy of the ChAdOx1 nCoV-19
940 (AZD1222) cOVID-19 vaccine against the B.1.351 variant in South Africa. *MedRxiv*. 2021;
941 doi: https://doi.org/10.1101/2021.02.10.21251247.
942 Mahase, E. (2021). Covid-19: Novavax vaccine efficacy is 86% against UK variant and 60%
943 against South African variant. *BMJ* 2021;372:n296
944 McCoy, A.J., Grosse-Kunstleve, R.W., Adams, P.D., Winn, M.D., Storoni, L.C., and Read,
945 R.J. Phaser crystallographic software. *J. Appl. Crystallogr. 2007;* ***40***: 658–674.
946 Pinto, D., Park, Y.J., Beltramello, M., Walls, A.C., Tortorici, M.A., Bianchi, S., Jaconi, S.,
947 Culap, K., Zatta, F., De Marco, A., et al. Cross-neutralization of SARS-CoV-2 by a human
948 monoclonal SARS-CoV antibody. *Nature* 2020; ***583***: 290–295.

949 Polack, F.P., Thomas, S.J., Kitchin, N., Absalon, J., Gurtman, A., Lockhart, S., Perez, J.L.,
950 Pérez Marc, G., Moreira, E.D., Zerbini, C., et al. Safety and Efficacy of the BNT162b2 mRNA
951 Covid-19 Vaccine. *N. Engl. J. Med*. 2020; **383**: 2603–2615.
952 Seemann, T., Lane, C.R., Sherry, N.L., Duchene, S., Gonçalves da Silva, A., Caly, L., Sait, M.,
953 Ballard, S.A., Horan, K., Schultz, M.B., et al. Tracking the COVID-19 pandemic in Australia
954 using genomics. *Nat. Commun*. 2020; **11**: 1–9.
955 Shang, J., Ye, G., Shi, K., Wan, Y., Luo, C., Aihara, H., Geng, Q., Auerbach, A., and Li, F.
956 Structural basis of receptor recognition by SARS-CoV-2. *Nature*. 2020; **581**: 221–224.
957 Skelly, D.T., Harding Sir William, A.C., Gilbert-Jaramillo Sir William, J., Knight Sir William,
958 M.L., Longet, S., Brown, A., Adele, S., Adland, E., Brown, H., and Stafford, L. (2021).
959 Vaccine-induced immunity provides more robust heterotypic immunity than natural infection
960 to emerging SARS-CoV-2 variants of concern. Research Square. 2021;
961 https://doi.org/10.21203/rs.3.rs-226857/v1.
962 Starr, T.N., Greaney, A.J., Dingens 1, A.S., and Bloom, J.D. (2021). Complete map of SARS-
963 CoV-2 RBD mutations that escape the monoclonal antibody LY-CoV555 and its cocktail with
964 LY-CoV016. B*ioRxiv*. 2021; https://doi.org/10.1101/2021.02.17.431683.
965 Stuart, D.I., Levine, M., Muirhead, H., and Stammers, D.K. Crystal structure of cat muscle
966 pyruvate kinase at a resolution of 2.6 Å. *J. Mol. Biol*. 1979; ***134*:** 109–142.Supasa, P., Zhou,
967 D., Dejnirattisai, W., Liu, C., Mentzer, A.J., Ginn, H.M., Zhao, Y., Duyvesteyn, H.M.E.,
968 Nutalai, R., Tuekprakhon, A., et al. (2021). Reduced neutralization of SARS-CoV-2 B.1.1.7
969 variant by convalescent and vaccine sera. *Cell*
970 2021;doi:https://doi.org/10.1016/j.cell.2021.02.033.
971 Tatusov, R.L., Galperin, M.Y., Natale, D.A., and Koonin, E. V. The COG database: A tool for
972 genome-scale analysis of protein functions and evolution. *Nucleic Acids Res*. 2000; **28:** 33–36.

973 Volz, E., Hill, V., McCrone, J.T., Price, A., Jorgensen, D., O'Toole, Á., Southgate, J., Johnson,
974 R., Jackson, B., Nascimento, F.F., et al. Evaluating the Effects of SARS-CoV-2 Spike Mutation
975 D614G on Transmissibility and Pathogenicity. *Cell*. 2021; ***184*:** 64-75.e11.
976 Voysey, M., Clemens, S.A.C., Madhi, S.A., Weckx, L.Y., Folegatti, P.M., Aley, P.K., Angus,
977 B., Baillie, V.L., Barnabas, S.L., Bhorat, Q.E., et al. Safety and efficacy of the ChAdOx1
978 nCoV-19 vaccine (AZD1222) against SARS-CoV-2: an interim analysis of four randomised
979 controlled trials in Brazil, South Africa, and the UK. *Lancet.* 2020; **397**: 99-111.
980 Walls, A.C., Park, Y.J., Tortorici, M.A., Wall, A., McGuire, A.T., and Veesler, D. Structure,
981 Function, and Antigenicity of the SARS-CoV-2 Spike Glycoprotein. *Cell*. 2020; **181**: 281-
982 292.e6.
983 Wang, P., Wang, M., Yu, J., Cerutti, G., Nair, M.S., Huang, Y., Kwong, P.D., Shapiro, L., *and*
984 *Ho, D.D.* Increased Resistance of SARS-CoV-2 Variant P.1 to Antibody Neutralization.
985 *bioRxiv* 2021; doi: https://doi.org/10.1101/2021.03.01.433466.
986 Wang, Q., Zhang, Y., Wu, L., Niu, S., Song, C., Zhang, Z., Lu, G., Qiao, C., Hu, Y., Yuen,
987 K.Y., et al. Structural and Functional Basis of SARS-CoV-2 Entry by Using Human ACE2.
988 *Cell*. 2020; **181**: 894-904.e9.
989 Wibmer, C.K., Ayres, F., Hermanus, T., Madzivhandila, M., Kgagudi, P., Oosthuysen, B.,
990 Lambson, B.E., de Oliveira, T., Vermeulen, M., van der Berg, K., et al. SARS-CoV-2 501Y.V2
991 escapes neutralization by South African COVID-19 donor plasma.
992 bioRxiv. 2021; doi: https://doi.org/10.1101/2021.01.18.427166
993 Winter, G. Xia2: An expert system for macromolecular crystallography data reduction. *J. Appl.*
994 *Crystallogr.* 2010; **43**: 186–190.
995 Winter, G., Waterman, D.G., Parkhurst, J.M., Brewster, A.S., Gildea, R.J., Gerstel, M.,
996 Fuentes-Montero, L., Vollmar, M., Michels-Clark, T., Young, I.D., et al. *DIALS*:

997 implementation and evaluation of a new integration package. *Acta Crystallogr. Sect. D Struct.*
998 *Biol*. 2018; **74**: 85–97.
999 Wu, Y., Wang, F., Shen, C., Peng, W., Li, D., Zhao, C., Li, Z., Li, S., Bi, Y., Yang, Y., et al.
1000 A noncompeting pair of human neutralizing antibodies block COVID-19 virus binding to its
1001 receptor ACE2. *Science.* 2020; ***368***: 1274–1278.
1002 Yuan, M., Liu, H., Wu, N.C., Lee, C.C.D., Zhu, X., Zhao, F., Huang, D., Yu, W., Hua, Y.,
1003 Tien, H., et al. (2020). Structural basis of a shared antibody response to SARS-CoV-2. Science.
1004 2020; **369**: 1119–1123.
1005 Zahradník, J., Marciano, S., Shemesh, M., Zoler, E., Chiaravalli, J., Meyer, B., Dym, O., Elad,
1006 N., and Schreiber, G. SARS-CoV-2 RBD in vitro evolution follows contagious mutation
1007 spread, yet generates an able infection inhibitor. *BioRxiv*. 2021;
1008 https://doi.org/2021.01.06.425392.
1009 Zhou, D., Duyvesteyn, H.M.E., Chen, C.P., Huang, C.G., Chen, T.H., Shih, S.R., Lin, Y.C.,
1010 Cheng, C.Y., Cheng, S.H., Huang, Y.C., et al. Structural basis for the neutralization of SARS-
1011 CoV-2 by an antibody from a convalescent patient. *Nat. Struct. Mol. Biol*. 2020; **27**: 950–958.
1012 Zhou, D., Dejnirattisai, W., Supasa, P., Liu, C., Mentzer, A.J., Ginn, H.M., Zhao, Y.,
1013 Duyvesteyn, H.M.E., Tuekprakhon, A., Nutalai, R., et al. (2021). Evidence of escape of SARS-
1014 CoV-2 variant B.1.351 from natural and vaccine induced sera. *Cell*. 2021;
1015 https://doi.org/10.1016/j.cell.2021.02.037.
1016 Zost, S.J., Gilchuk, P., Case, J.B., Binshtein, E., Chen, R.E., Nkolola, J.P., Schäfer, A., Reidy,
1017 J.X., Trivette, A., Nargi, R.S., et al. Potently neutralizing and protective human antibodies
1018 against SARS-CoV-2. Nature 2020; **584**: 443–444.
1019

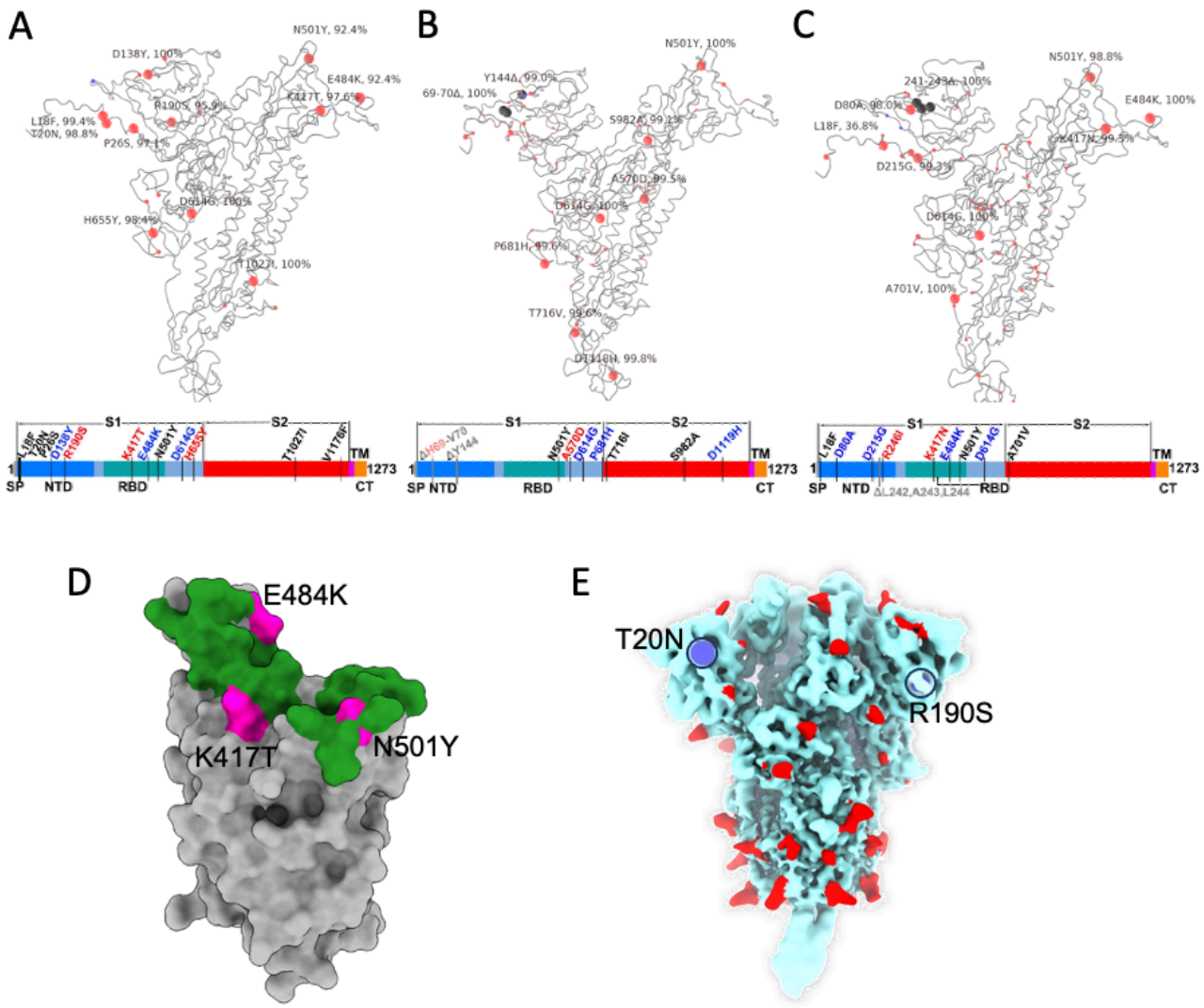
A
N501Y, 92.4%
D138Y, 100%
E484K, 92.4%
K417T, 97.6%
R190S, 95.9%
L18F, 99.4%
T20N, 98.8%
P26S, 97.1%
D614G, 100%
H655Y, 98.4%
T1027I, 100%
B
N501Y, 100%
Y144Δ, 99.0%
69-70Δ, 100%
S982A, 99.1%
A570D, 99.5%
D614G, 100%
P681H, 99.6%
T716V, 99.6%
D1118H, 99.8%
C
N501Y, 98.8%
241-243Δ, 100%
D80A, 98.0%
E484K, 100%
L18F, 36.8%
K417N, 99.3%
D215G, 99.3%
D614G, 100%
A701V, 100%
S1
S2
TM
1
1273
SP
NTD
RBD
CT
D
E484K
K417T
N501Y
E
T20N
R190S

Figure1

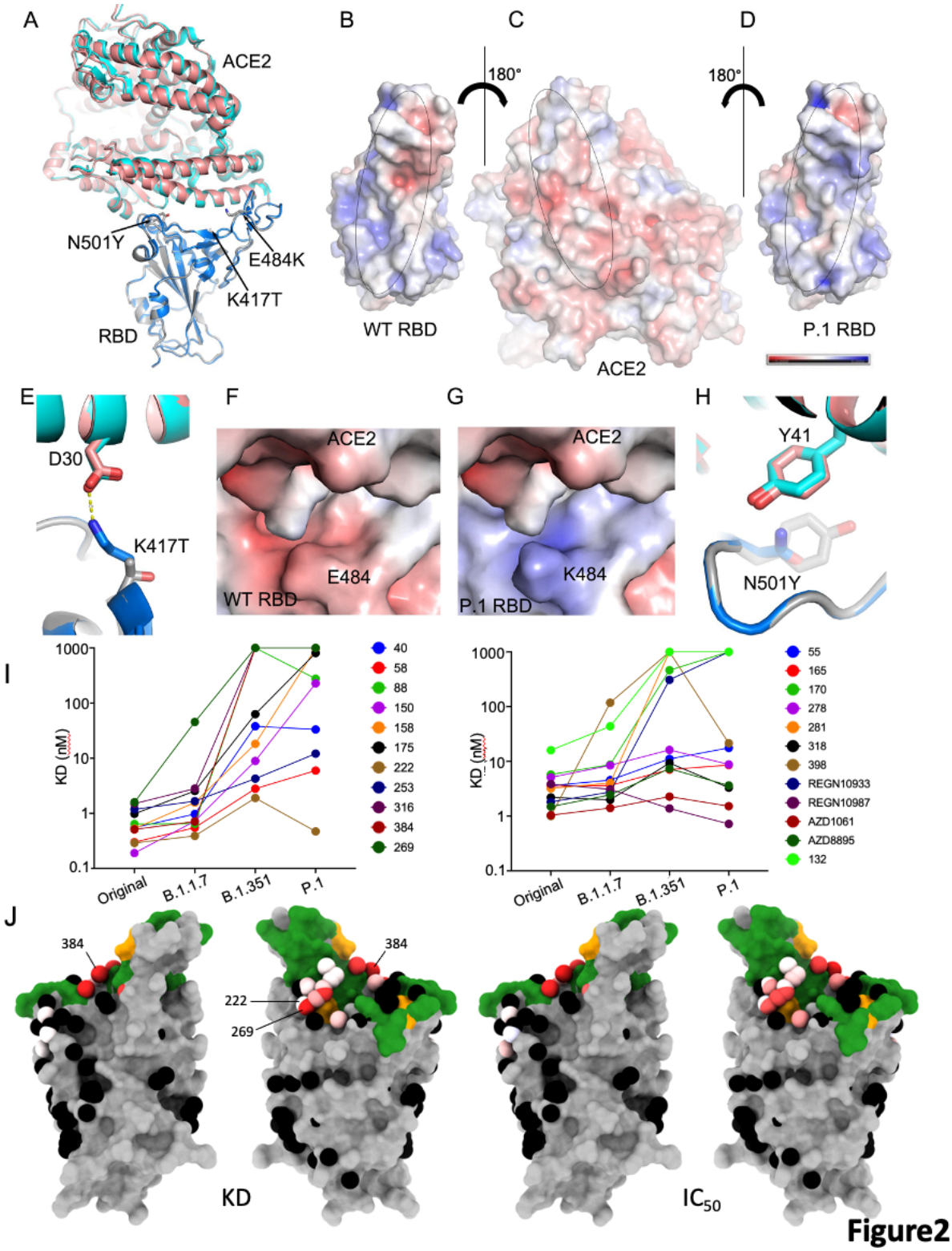
A
ACE2
N501Y
E484K
K417T
RBD
B
C
D
180°
180°
WT RBD
ACE2
P.1 RBD
E
D30
K417T
F
ACE2
E484
WT RBD
G
ACE2
K484
P.1 RBD
H
Y41
N501Y
I
KD (nM)
1000
100
10
1
0.1
Original
B.1.1.7
B.1.351
P.1
40
58
88
150
158
175
222
253
316
384
269
55
165
170
278
281
318
398
REGN10933
REGN10987
AZD1061
AZD8895
132
J
384
222
269
KD
IC50

Figure2

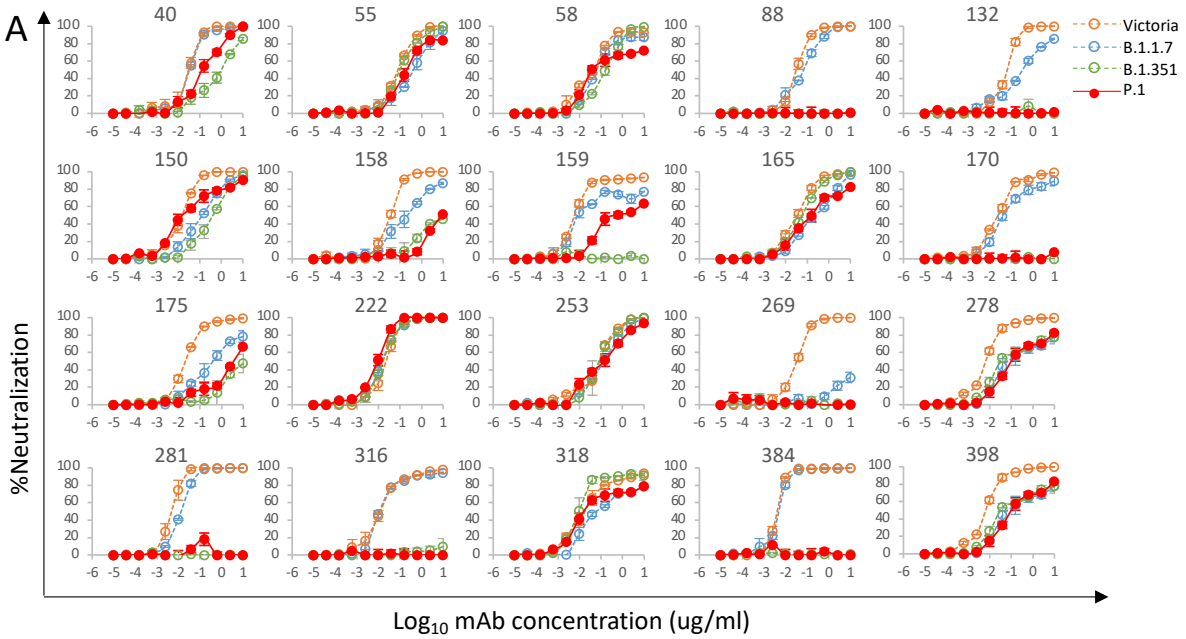

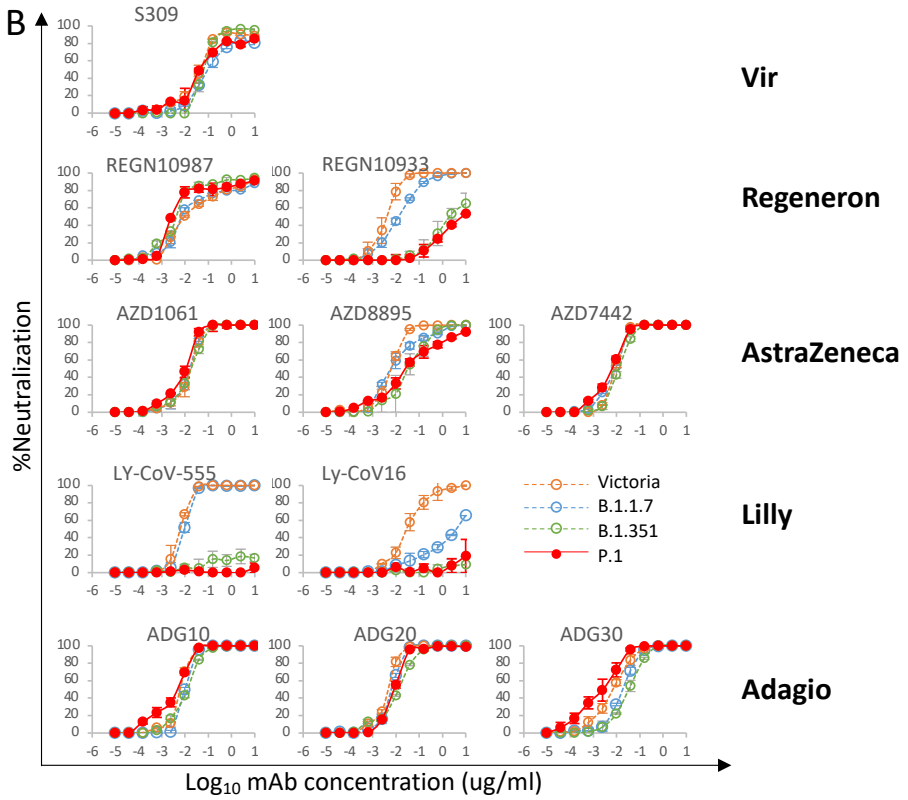

Figure3

1024

1025

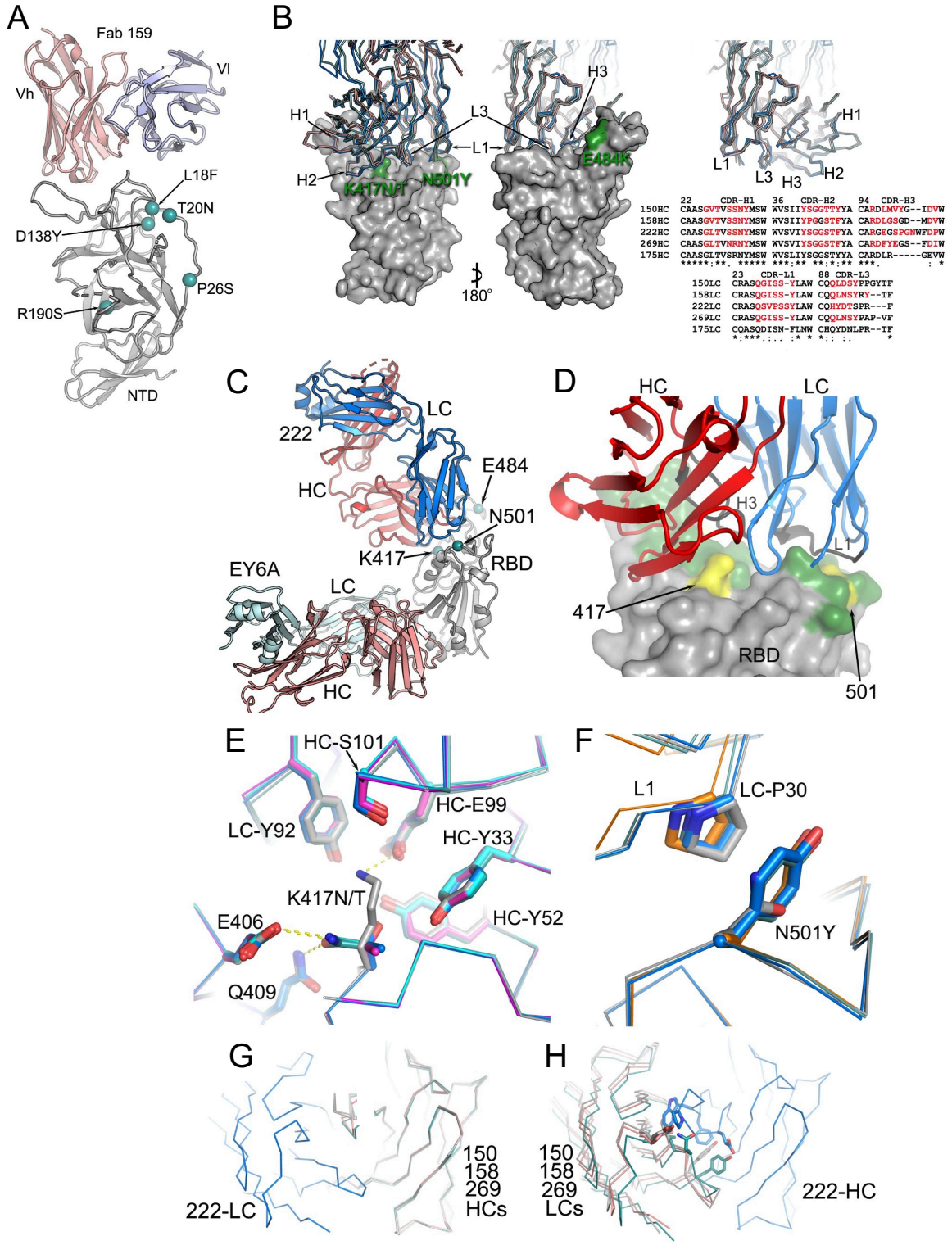

Figure4

1026

1027

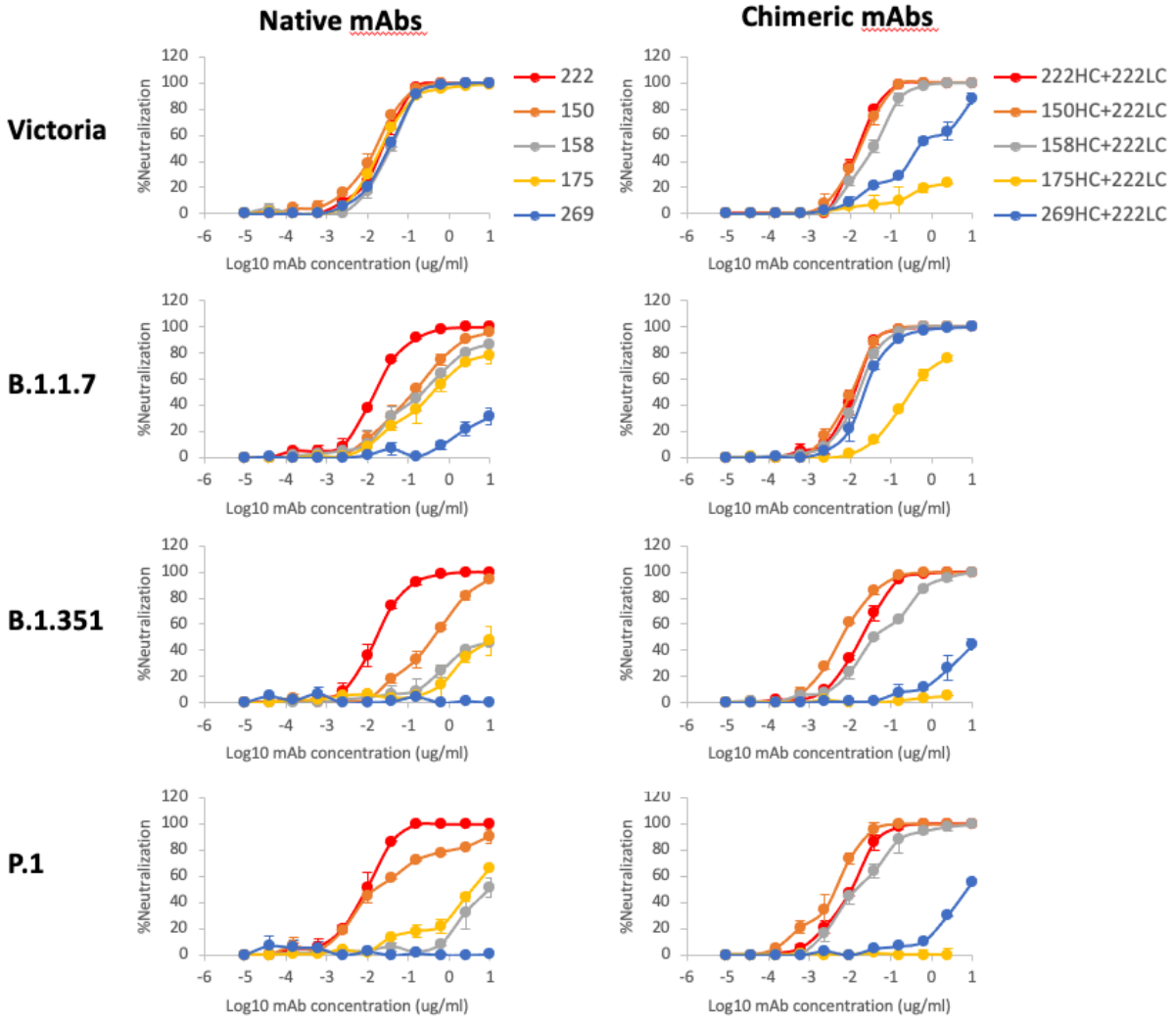

1028

1029

Figure5

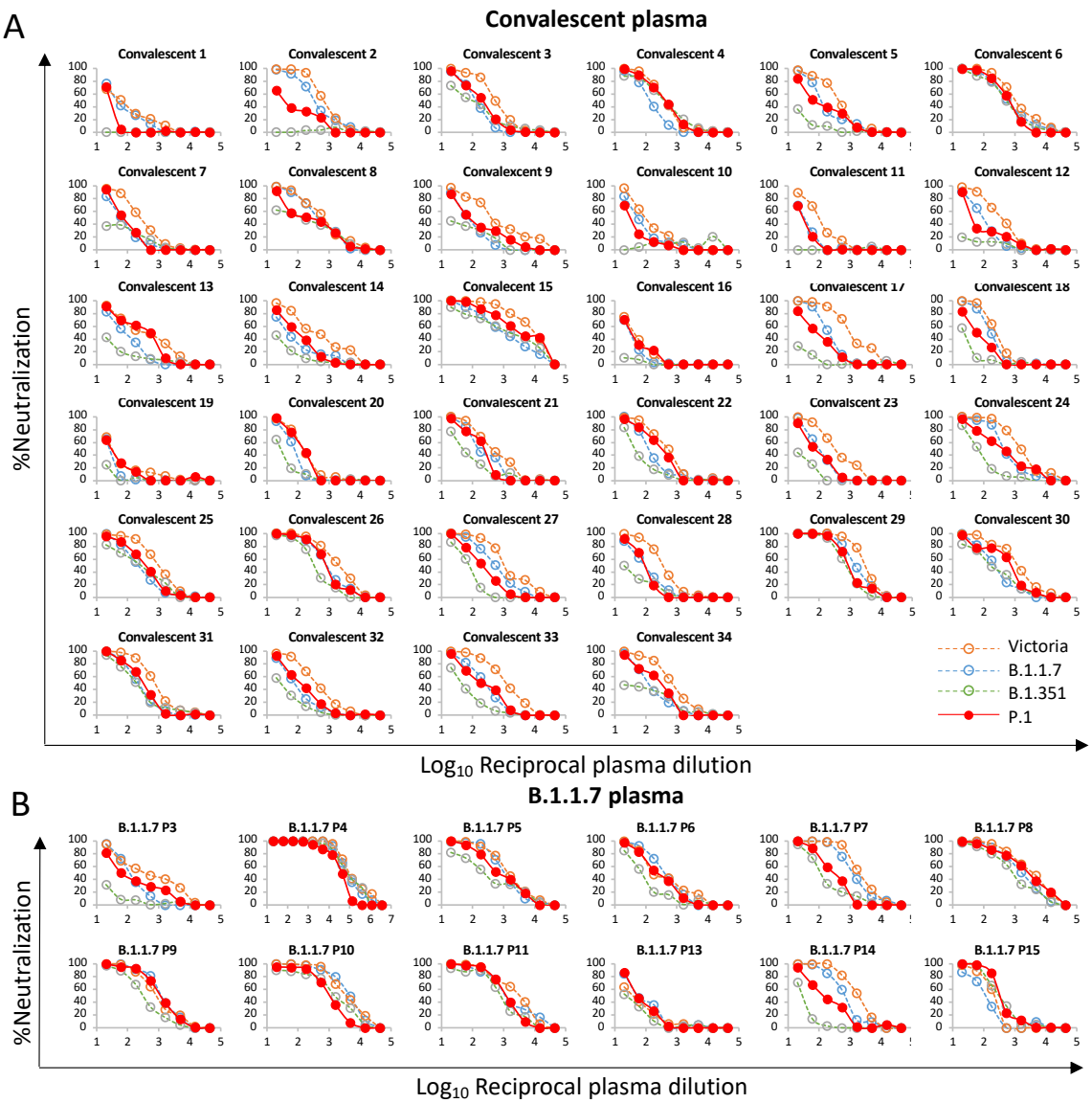
A
Convalescent plasma
%Neutralization
Log10 Reciprocal plasma dilution
Victoria
B.1.1.7
B.1.351
P.1
B
B.1.1.7 plasma
%Neutralization
Log10 Reciprocal plasma dilution

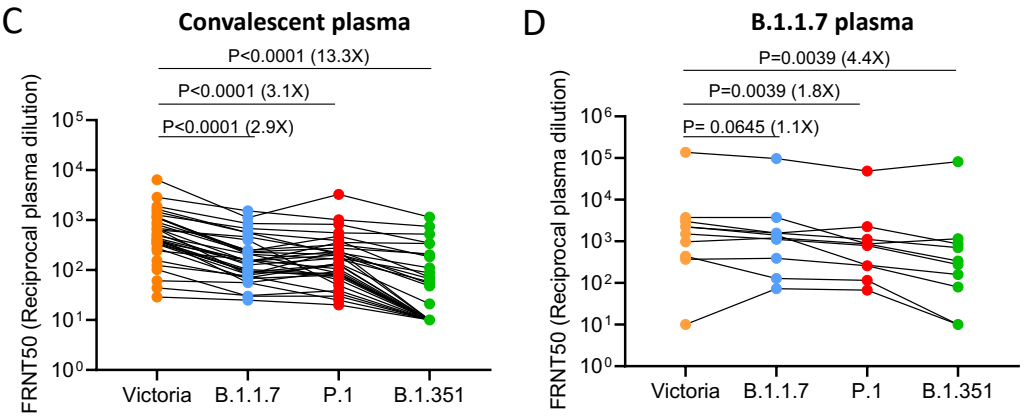
C
Convalescent plasma
P<0.0001 (13.3X)
P<0.0001 (3.1X)
P<0.0001 (2.9X)
FRNT50 (Reciprocal plasma dilution)
Victoria
B.1.1.7
P.1
B.1.351
D
B.1.1.7 plasma
P=0.0039 (4.4X)
P=0.0039 (1.8X)
P= 0.0645 (1.1X)
FRNT50 (Reciprocal plasma dilution)
Victoria
B.1.1.7
P.1
B.1.351

Figure6

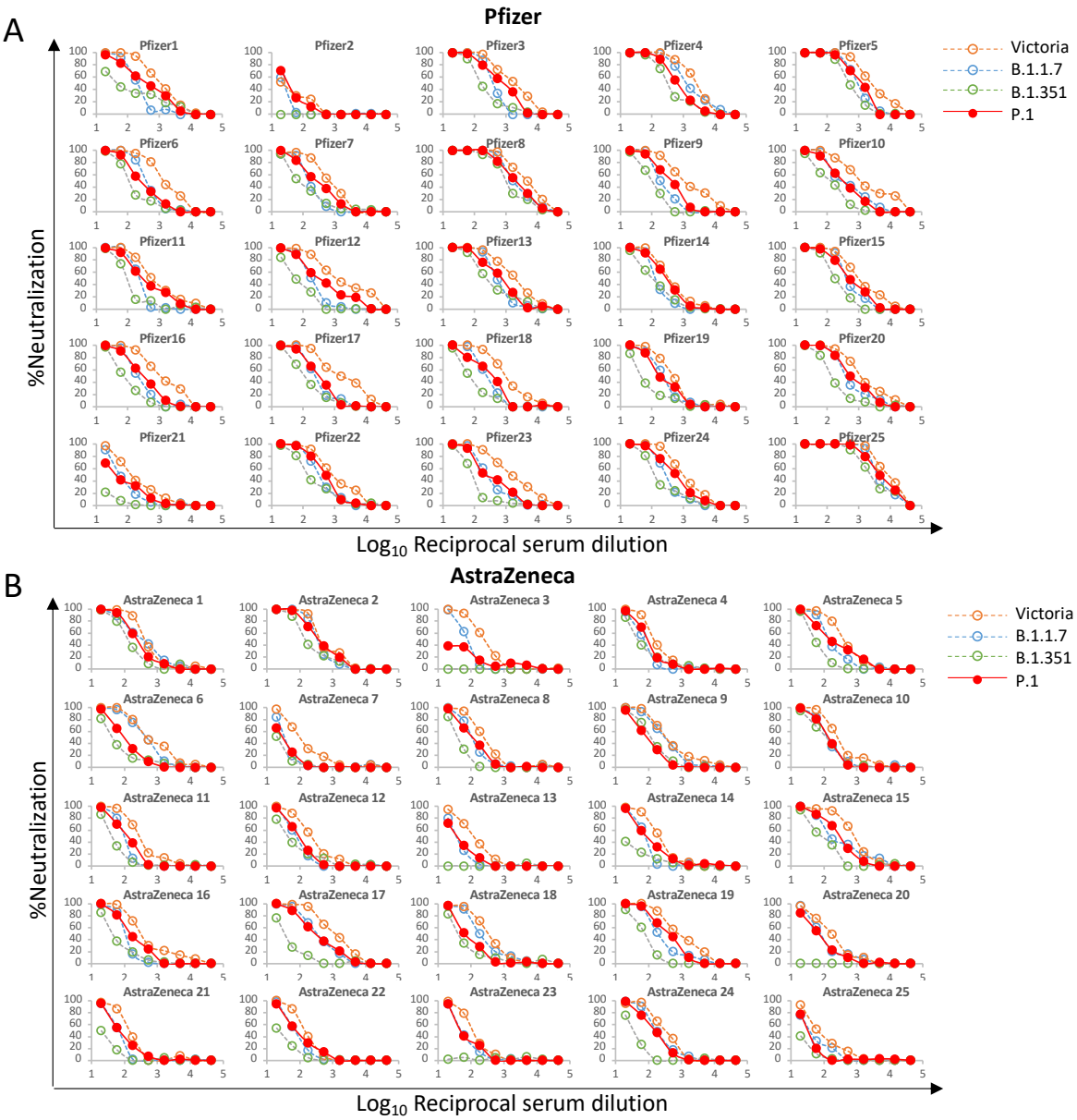

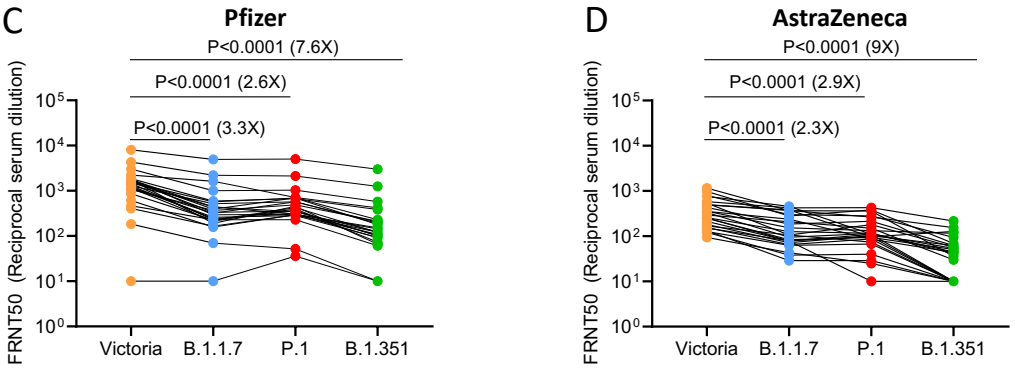

Figure7

1032